AD-A064 443 ROCKWELL INTERNATIONAL THOUSAND OAKS CALIF SCIENCE --ETC F/G 11/6
ENVIRONMENTAL EFFECTS ON FATIGUE CRACK INITIATION.(U)
FEB 79 W L MORRIS, O BUCK N00014-76-C-0452
UNCLASSIFIED SC5050.1FR NL

1 OF 2
AD
A064443

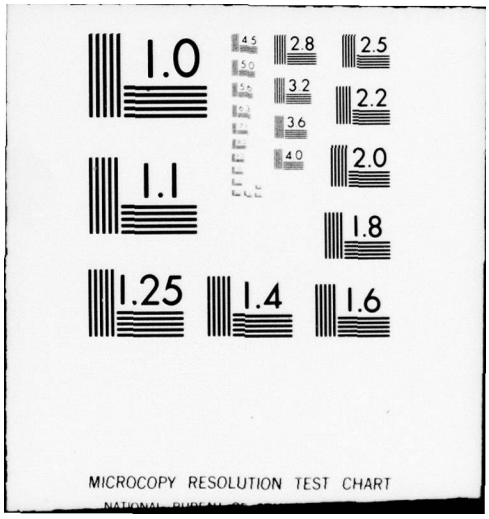
1.0
1.1
1.25
1.4
1.6
1.8
2.0
2.2
2.5
2.8
3.2
3.6
4.0
4.5
5.0
MICROCOPY RESOLUTION TEST CHART

LEVEL II

SC5050.1FR
COPY NO. 10

ENVIRONMENTAL EFFECTS ON FATIGUE CRACK INITIATION

Final Report
Contract No. N00014-76-C-0452
For period 12/01/75 through 11/30/78

Submitted to:

Director, Metallurgy Programs
Material Sciences Division
Office of Naval Research
800 North Quincy Street
Arlington, Virginia 22217

Prepared by:

W. L. Morris and O. Buck

"This research was sponsored by the Office of Naval Research under Contract No. N00014-76-C-0452. (Project No. 471)."

Rockwell International
Science Center

UNCLASSIFIED

SECURITY CLASSIFICATION OF THIS PAGE (When Data Entered)

REPORT DOCUMENTATION PAGE

READ INSTRUCTIONS BEFORE COMPLETING FORM

1. REPORT NUMBER

2. GOVT ACCESSION NO.

3. RECIPIENT'S CATALOG NUMBER

(9) Final Rept. 1 Dec 75-30 Nov 78,

4. TITLE (and Subtitle)

(6) Environmental Effects on Fatigue Crack Initiation

5. TYPE OF REPORT & PERIOD COVERED

Final Report, 12/01/75 through 11/30/78

6. PERFORMING ORG. REPORT NUMBER

(14) SC5050.1FR

7. AUTHOR(s)

(10) W. L. Morris [redacted] O. Buck

8. CONTRACT OR GRANT NUMBER(s)

(15) N00014-76-C-0452

9. PERFORMING ORGANIZATION NAME AND ADDRESS

Rockwell International, Science Center
1049 Camino Dos Rios
Thousand Oaks, Calif. 91360

10. PROGRAM ELEMENT, PROJECT, TASK AREA & WORK UNIT NUMBERS

~~471~~ (NR 036-113)

11. CONTROLLING OFFICE NAME AND ADDRESS

Director, Metallurgy Programs, Material Sciences Div.
Office of Naval Research, 800 No. Quincy Street
Arlington, VA 22217 (ATTN: Dr. P.A. Clarkin, Code 471)

12. REPORT DATE

(11) Feb[redacted]79

13. NUMBER OF PAGES

~~83~~ (12) 101p.

14. MONITORING AGENCY NAME & ADDRESS (if different from Controlling Office)

15. SECURITY CLASS. (of this report)

Unclassified

15a. DECLASSIFICATION/DOWNGRADING SCHEDULE

16. DISTRIBUTION STATEMENT (of this Report)

Approved for public release; distribution unlimited

17. DISTRIBUTION STATEMENT (of the abstract entered in Block 20, if different from Report)

18. SUPPLEMENTARY NOTES

19. KEY WORDS (Continue on reverse side if necessary and identify by block number)

Fatigue, cracking, failure, fatigue life, fatigue properties, ductility, surface defects, crack initiation, aluminum alloys, corrosion environments, plastic theory, computerized simulation, Monte Carlo method

20. ABSTRACT (Continue on reverse side if necessary and identify by block number)

Models of microscopic failure mechanisms important to the crack initiation stage of the fatigue failure of aluminum alloys have been proposed and verified. Included are: (1) a model relating rate of nucleation of surface microcracks at intermetallic particles to particle and grain size and ambient humidity; (2) and models which relate rate of growth of surface microcracks, with lengths of approximately the grain size, to the alloy microstructure in

DD FORM 1 JAN 73 1473 EDITION OF 1 NOV 65 IS OBSOLETE

UNCLASSIFIED

SECURITY CLASSIFICATION OF THIS PAGE (When Data Entered)

389949

20. the region of a nucleation site and to ambient humidity. The models have been used to develop a Monte Carlo simulation of the fatigue failure of aluminum alloys which can be used to predict the effect of alloy microstructure and environmental humidity on: (1) mean and scatter in fatigue lifetime; (2) microscopic parameters such as numbers and lengths of microcracks, and microcrack closure stresses. Simulated and measured fatigue behavior are compared for several aluminum alloys.

CONTENTS

CONTENTS

LIST OF ILLUSTRATIONS

LIST OF ILLUSTRATIONS

LIST OF ILLUSTRATIONS

1.0 INTRODUCTION AND ABSTRACT

This is the final report on Contract No. N00014-76-C-0452: "Environmental Effects on Fatigue Crack Initiation." The purpose of the research was to develop models which describe the effect of humidity on microscopic fatigue failure processes in aluminum, and lead to a description of the scatter in fatigue lifetime which results from the statistical nature of the fatigue failure process. In order to develop a comprehensive model, spanning all the sequencial failure mechanisms of importance for at least one alloy, we restricted the scope of our research to alloy and loading parameters as follows:

1) To materials for which principal crack nucleation occurs at or near the the surface at intermetallic particles - such as is the case for 2000 and 7000 series aluminum alloys.

2) To peak hardness or overaged alloys.

3) For constant cyclic amplitude, $R = \sigma_{min}/\sigma_{max} = -1$, and with maximum amplitude less than the alloy's 0.2% yield strength.

4) To sinusoidal loading with frequencies in the range 1 - 5 Hz.

5) To materials relieved of macroscopic (or long range) residual surface stress.

Our research addressed mechanisms in the initiation stage of fatigue failure. Here we use initiation to refer to all processes prior to the formation of a terminal crack (of sufficient size) whose subsequent propagation can be predicted by conventional fracture mechanics. For the

aluminum alloys studied initiation is comprised of three processes not heretofore described by fracture mechanics:

1) Nucleation - The formation of a microcrack, typically at an intermetallic particle site.

2) Early Microcrack Growth - The growth of cracks with lengths on the order of the grain size, with propagation rate substantially influences by the presence of grain boundaries.

3) Coalescence - The linking of microcracks to form a terminal crack.

Analytical models of processes 1 and 2 have been developed and are the basis for a Monte-Carlo simulation of fatigue failure devised to predict the lifetime time properties of the aluminum alloys of interest. In the computer simulation we nucleate surface microcracks which grow according to rules derived from the models. The variation in lifetime from specimen to specimen is related to statistical fluctuations in alloy microstructure from specimen to specimen. The statistical effect of crack coalescence on lifetime enters the simulation from variation in relative locations of the microcracks. In Section 2.0 we describe, in outline form, the general sequence of events observed in fatigue failure of 2000 and 7000 series aluminum alloys of interest, and the role of humidity in the failure process. In Section 3.0, detailed experimental results are discussed along with their mechanistic implications. Finally, in Section 4.0, results of modeling predictions are compared to experimental data.

2.0 OUTLINE OF FATIGUE FAILURE SEQUENCE TO BE MODELED

Nucleation

Crack nucleation, for cyclic loading, occurs as the result of accumulated damage due to microplastic deformation of the alloy. Owing to lack of bulk constraint of deformation, the surface is the most vulnerable place for crack nucleation. Exceptions, wherein subsurface nucleation is possible include: 1) presence of a compressive residual stress at the surface; or 2) presence of large subsurface discontinuities (voids, inclusions) which can act as sites for crack nucleation.

The rate of crack nucleation at the surface is influenced by the type and size of discontinuities at or near the surface which can act as stress concentrators, and hence, as sites for nucleation. In the alloys of interest, intermetallic particles in size range 5 - 40 μm are common nucleation sites. Occasional nucleation of cracks at grain boundaries is also observed, however, and it is known that, even in the absence of any initial surface discontinuities, cracking can ultimately begin as the result of an intrusion/extrusion type mechanism. It is a weakest link criteria which governs which of the several modes of crack nucleation will dominate [R1].

For a given surface discontinuity, the number of fatigue cycles required for nucleation is determined by achievement of a critical strain energy density in the region of the discontinuity. Cycles to nucleation are reduced if the discontinuity size is large, if the discontinuity is found within a large grain permitting large slip distances, and if the crystallographic orientation of the grain is favorable [R2]. During fatigue, ductility and hence propensity to further microplastic deformation of the alloy surface layer changes. For the peak hardness alloys studied, the trend, due to cutting of precipitates, is for the surface to soften. In the presence of humidity, however, surface ductility is decreased over that found for dry air. As a consequence, one observes a reduced rate of crack nucleation at intermetallic sites at elevated humidity. Humidity can also directly alter the properties of the discontinuity itself leading to further complexity. In

Al 2219-T851, for instance, an observed effect of humidity is to embrittle the interface between intermetallic and matrix [R1]. An additional complexity ignored in the present research is the effect of microscopic residual strain fields associated with discontinuites, which are present in the as received material.

In Section 3.0 we discuss the final status of our modeling of nucleation phenomena. This includes: (1) test of an analytical relationship between minimum cycles to nucleation and the intermetallic size, the size of the grain containing the intermetallic, and the cyclic stress amplitude; (2) a method for measuring the effect of humidity on ductility of the surface layer of an alloy, and (3) observations on interrelationships among intermetallic composition, structure, relative humidity and the propensity to nucleate cracks at intermetallic particle sites.

Early Microcrack Growth

The rate of propagation of surface microcracks is substantially smaller, on an average, than expected from conventional fracture mechanics. We find that the retarded growth is principally the result of large positive crack closure stresses developed by the microcracks. Here we use closure stress in a generic sense to refer to all processes which lead to a reduced cyclic plastic deformation per cycle at the crack tip. We relate the rate of growth of the microcracks to an effective stress intensity range, ΔK_{eff}, where $\Delta K_{eff} \propto (\sigma_{max} - \sigma_{cc})$, (i.e., the cyclic stress range, the maximum stress minus the closure stress).

The closure stress, σ_{cc}, for a given crack is a function of location along the crack front and changes as the crack grows, leading to fluctuations in growth rate. Three independent phenomena lead to positive values of σ_{cc}, and it is the mechanism which produces the largest σ_{cc} at a given point on the crack front which determines σ_{cc} at that point and that instant. The three mechanisms are:

1) Contact of the opposing fracture surface in the region of the intermetallic particle. The contact is apparently the result of a change in shape of the fractured intermetallic particle. σ_{cc} resulting from this mechanism is independent of the maximum cyclic amplitude, σ_{max}. Closure from the mechanism is of greatest importance when the microcrack is of a size close to the intermetallic from which has nucleated. As the crack grows $\sigma_{cc} \propto (2c)^{-1}$, where 2c is the crack length.

2) Contact of opposing fracture surfaces due to fracture surface roughness. We have not studied this mechanism in detail, but find that it sets a lower limit on σ_{cc} of ≈ 0.2 σ_{max}.

3) Residual tensile strain at the crack tip. The tensile strain develops as the result of an incomplete reversal of plastic deformation at the crack tip. The mechanism dominates the closure stress phenomena for all but the earliest stage of growth of microcracks.

An important difference between microcrack growth and crack growth in fracture mechanics specimens is that for microcracks the plastic zone size is not as predicted by continuum analysis. Instead, the plastic zone size is principally limited by the distance between a microcrack tip and the next neighboring grain boundary. By a series of experiments, we show in Section 3.0 that the grain size at the crack tip can be used to predict σ_{cc}, arising from residual strain at the crack tip, and hence, microcrack propagation rate. We show that a direct effect of humidity is to reduce σ_{cc} and so lead to increased crack propagation rate.

An additional complication should also be noted. While crack closure stresses are the prime factor in microcrack growth, closure stress affects

only Mode I (i.e., tensile opening) crack propagation. As a consequence, if $\sigma_{cc} \approx \sigma_{max}$ it is not uncommon to observe Mode II propagation. This is more common in the grain of initiation where the crack is under the influence of a large closure stress from the intermetallic initiation site. It is also observed as a microcrack begins to propagate into an exceptionally large grain, for which the residual tensile strain developed at the crack tip is large. Propagation typically reverts to Mode I as the closure stress drops.

3.0 SUMMARY OF EXPERIMENTS AND MODELS CONCERNING CRACK NUCLEATION AND EARLY MICROCRACK PROPAGATION

Nucleation

The common site for nucleation of cracks at an intermetallic particle is at the interface between the matrix and the intermetallic proper. Nucleation is observed at the circumference of spherical intermetallics (Fig. 1) and also interior to particles containing lamina of matrix material, such as in the example in Fig. 2 for Al 2219-T851. In the latter case, cracking commonly begins within the particle at the matrix-lamina interface. In the 2000 and 7000 series aluminum alloys the laminated internal structure of the intermetallic particles is found in association with particles which have been present during rolling (i.e. which are elongated in the rolling direction). The laminae lie approximately perpendicular to the rolling direction (R.D.) and fracture at the lamina-intermetallic interface occurs only for loading in the R.D. As a consequence, low Fe content Al 2219-T851, which contains few spherical intermetallics, has a substantially longer fatigue life when the loading axis is in the long transverse direction. Crack nucleation leading to failure occurs at grain boundaries. For Al 2219-T851 the intermetallic particle structure is related to particle composition, which also affects the sensitivity of the particles to crack nucleation as a function of humidity. Our observations on the interrelationships among particle composition, structure, humidity, and propensity to nucleation of microcracks have been reported in detail elsewhere.[D1]

A theoretical expression to relate the minimum number of fatigue cycles to crack nucleation at intermetallic particles to the alloy microstructure in the vicinity of a particle has been developed with support of Rockwell IR&D funds.[R2] The main result of the analysis is that the minimum number of cycles to nucleation, N, is given by

SC78-153

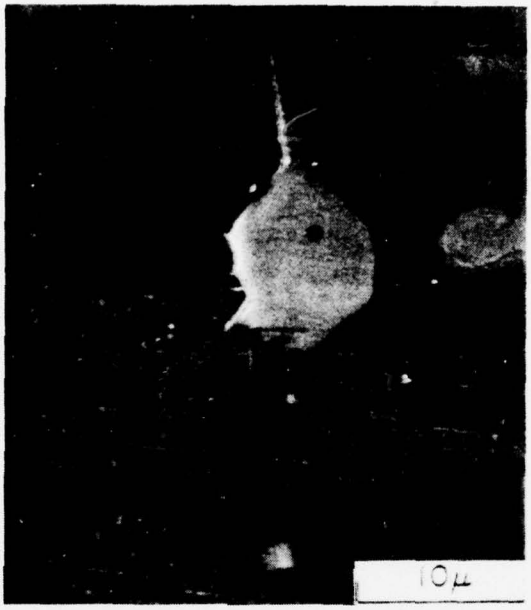

Fig. 1 Circumferential crack at θ phase particle in Al 2219-T851.

SC78-157

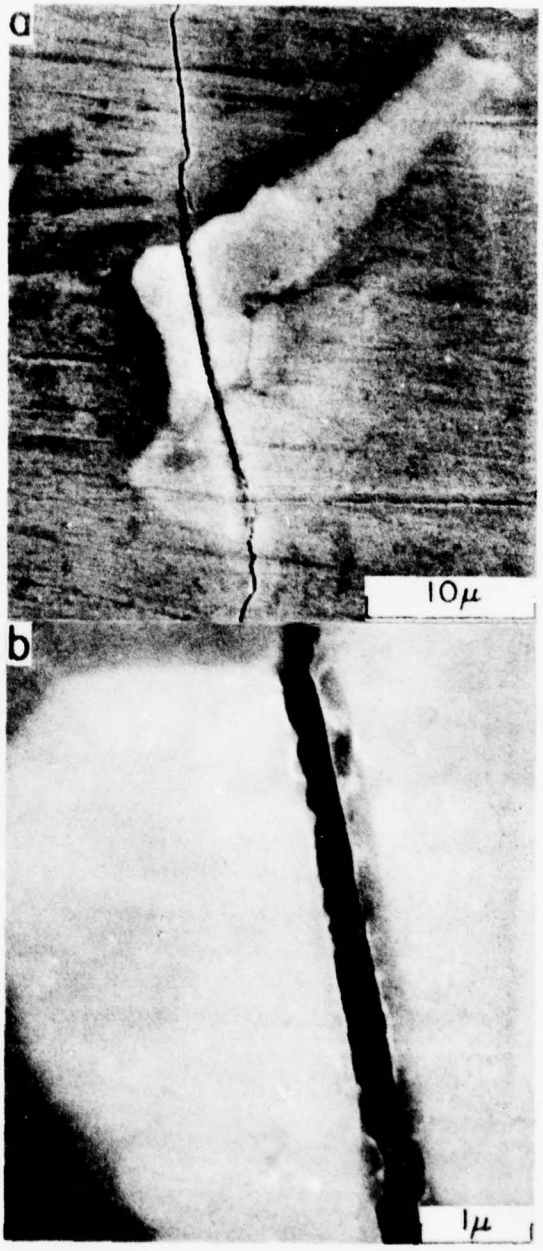

Fig. 2 Crack at internal lamina in β phase particle in Al 2219-T851.

$$N = \frac{C_o}{\sqrt{WD}^2(\sigma_{max} - \sigma_o)^2} \quad . \qquad (1)$$

C_o and σ_o are material constants. As illustrated by Fig. 3, W is the width of the intermetallic normal to the principal stress axis, D is the maximum distance of slip along the surface at approximately 45° to the principal stress. The model distinguishes two steps to crack nucleation; (a) formation of a crack inside to the intermetallic; (b) propagation into the matrix. In instances of surface pitting by corrosion, step (a) presumably is not required, and the analysis suggests that in any case step (b) is rate controlling for all but the lowest cyclic stress. Equation 1 describes step (b). As the effect of crystallographic orientation has been ignored in the analysis, Eqn. (1) is expected to be a lower bound of the number of cycles to nucleation, with larger N occurring for less favorable orientations. In the future a more complete theory must also consider the effect of triaxial constraints on N.

We have tested Eqn. (1) with ONR support by comparison to experimental results obtained for Al 2219-T851.[D2] Plotted in Fig. 4 are W vs D values for nucleation at intermetallic particles approximately occurring at three increments in fatigue cycles, N, as indicated. Polished flexural fatigue specimens of Al 2219 utilized were given a light chemical etch so that the grain boundaries could be observed in a scanning electron microscope (SEM). Dashed lines in Fig. 4a-c are a fit of Eqn. (1) to a single W, D value, (x), in the upper right corner of 4a. As expected, Eqn. (1) defines a lower bound of the data. The scatter towards larger W, D values is attributed principally to variation in crystallographic orientation from grain to grain.

While these are preliminary results, they do suggest the utility of Eqn. (1) in describing the effect of discontinuity size, and grain size on cycles to crack nucleation. We also know that, at least qualitatively, the stress dependence of the expression is good. Before similar experiments are done to rigorously test the expression, however, the desire is to incorporate the effect of crystallographic orientation into the expression. Currently, in

SC78-2960

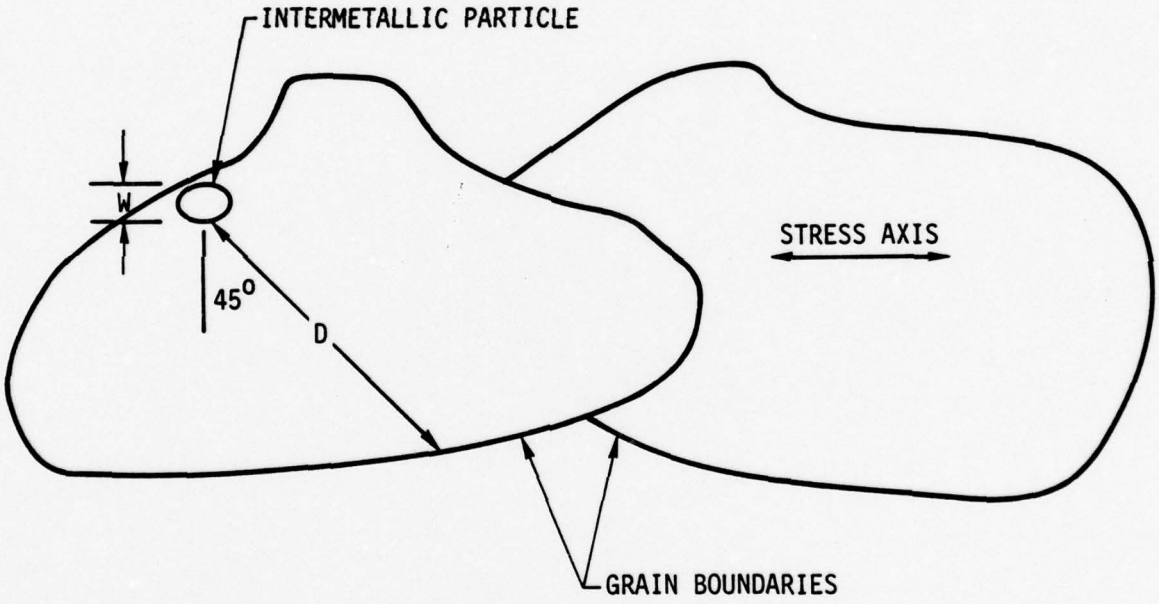

Fig. 3 Intermetallic width and slip distance parameters important to crack nucleation.

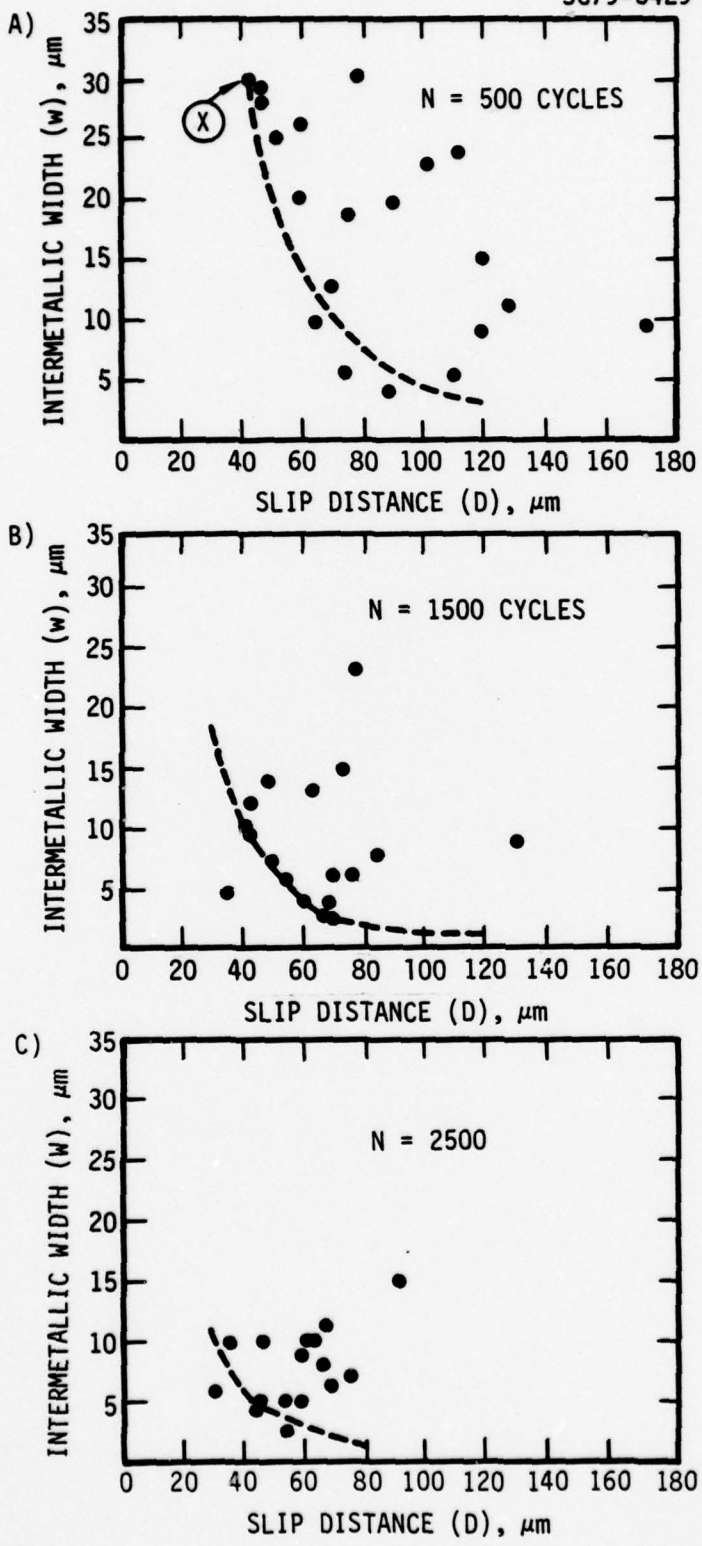

Fig. 4 Range of intermetallic widths and slip distances leading to nucleation for three increments in fatigue for Al 2219-T851.

research supported by Rockwell, we are approaching this with a Monte Carlo simulation, by replacing σ_{max} with an effective surface stress which is a function of the orientation of the <111> type slip planes in a grain relative to the external stress axis. Computer generated scatter plots similar to those of Fig. 4 have already been obtained with the technique.

Early Microcrack Growth

The first indirect evidence of the large closure stresses developed by microcracks was the observation that the surface microcracks in Al 2048 and Al 2219 did not completely close upon relaxation of external load. [D3,4]. It was also noted that the residual crack openings were particularly large if the cracks were of grain size, suggesting that the closure stress increased as crack lengths reach the grain size - consistent with observed retardation in cracking rate. A method was developed to determine the "average" closure stress of a microcrack by a compliance measurement.[D4] Using a miniature flexural fatigue specimen (Fig. 5) the opening of microcracks was measured as a function of surface stress giving results as those illustrated in Fig. 6. "Closure" defined by Fig. 6 is considered to be an average for the crack in that it is known that the true closure stress is a function of location along the crack front. Hereafter we refer to the average closure stress determined by such a measurement as $\overline{\sigma}_{cc}$.

In a search for the fundamental mechanisms of closure for microcracks a series of experiments were done to relate $\overline{\sigma}_{cc}$ to the shape of microcracks and to crack opening parameters as a function of crack length. Two regions of crack closure behavior were distinguished:

a) Short cracks for which crack length was less than a factor of two larger than the width of the intermetallic from which nucleation took place. In this circumstance, $\overline{\sigma}_{cc}$ was found to be independent of σ_{max}. Crack closure resulted from a misfit of fracture surfaces in the region of the intermetallic.

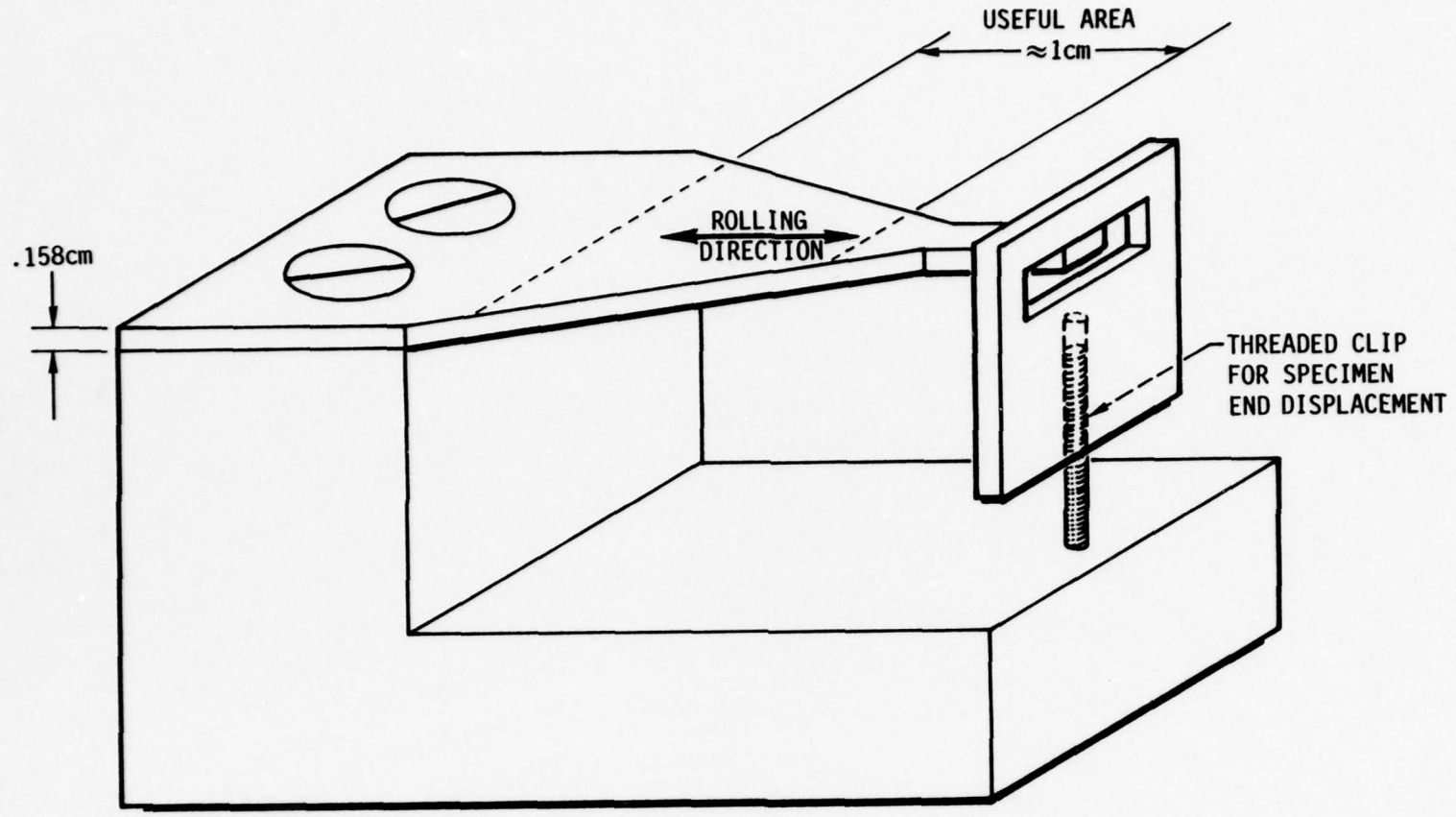

Fig. 5 Schematic illustration of jig used for loading of a miniature flexure specimen in an SEM.

SC78-387

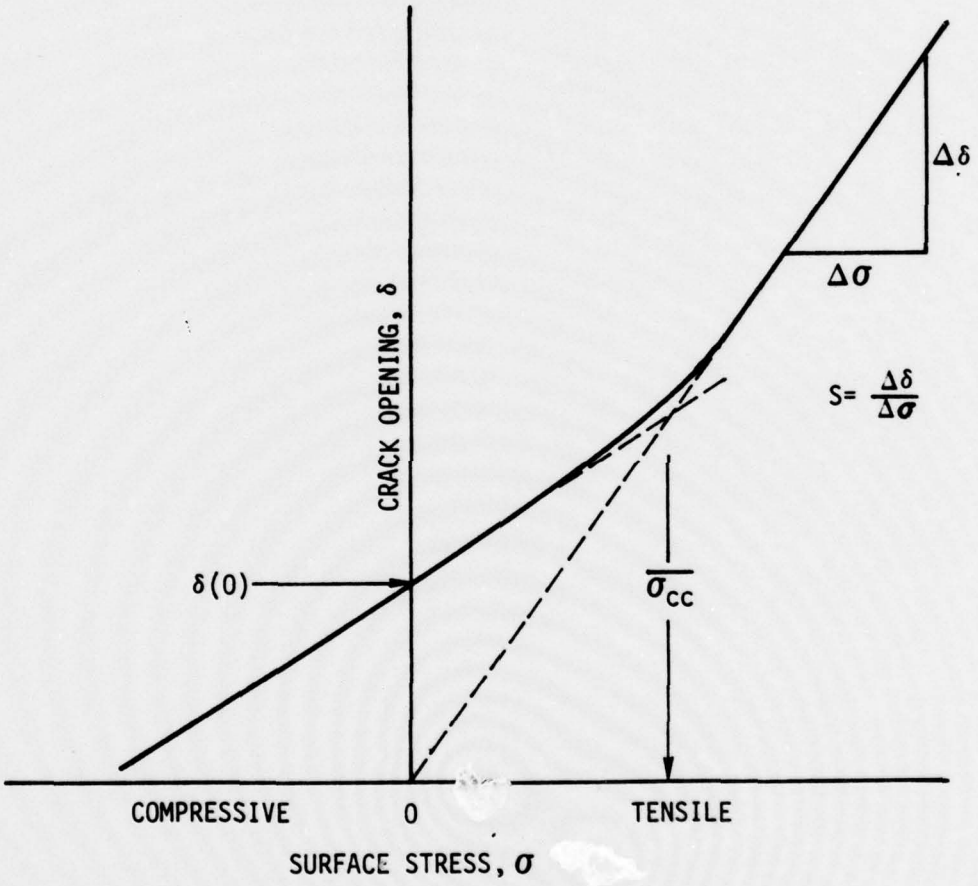

Fig. 6 Typical dependence of crack opening displacement on surface stress, illustrating the definition of the average crack closure stress, $\bar{\sigma}_{cc}$.

b) Longer microcracks for which

$$\bar{\sigma}_{cc} = C' \frac{\delta(o)}{\delta(\sigma_{max})} \sigma_{max} \qquad (2)$$

C' is a material constant and $\delta(o)/\delta(\sigma_{max})$ is the ratio of opening at the crack center at zero and maximum stress, respectively. Closure in this case is attributed to residual tensile strain at the crack tip. For a given crack, $\delta(o)/\delta(\sigma_{max})$ is a constant and hence $\bar{\sigma}_{cc}$ is a fixed fraction of σ_{max}. The measurements leading to these conclusions have been reported in Met. Trans.[D4-7]

While determination of $\bar{\sigma}_{cc}$ sufficed to define mechanisms and trends in closure development with microcrack growth, it was necessary to develop quantitative procedures to measure the true closure stress as a function of location along the crack front, as a means to define and test quantitative models of microcrack growth. Three series of experiments are described in 3.1-3.3.

a) It was shown that the crack closure stress, σ_{cc}, at a surface crack tip arising from residual tensile strain could be determined quantitatively from measurement of crack tip opening displacement (CTOD).[D8]

b) Comparison between rate of microcrack growth dc/dN, and an effective stress intensity range, $\Delta K_{eff} \propto (\sigma_{max} - \sigma_{cc})$ was made for Al 2219-T851. σ_{cc} was determined at increments in crack growth by CTOD measurements. We found that

$$\frac{dc}{dN} = A(\Delta K_{eff})^m \qquad (3)$$

gave a good prediction of the microcrack growth rate, where A and m are material constants.[D9]

c) An essential element of the deformation process for microcracks is that the plastic zone size is not as predicted from continuum mechanics. Instead the zone of significant deformation is determined by grain boundary constraints and for simple grain shapes can be predicted from the distance of the crack tip to the next grain boundary (Fig. 7). Thus

$$\sigma_{cc} = \alpha \frac{z_o}{2c} \sigma_{max} \quad , \qquad (4)$$

where α is a material constant which is sensitive to humidity.[D10] First evidence for the non-continuum nature of the crack tip deformation was published in Met. Trans.[D7] In 3.1-3.2 we expand upon the discussion of the phenomena, concluding in 3.3 a comparison between CTOD and distance of crack tip to grain boundary which is the basis for Eqn. (4).

3.1 RELATIONSHIP OF SURFACE MICROCRACK TIP OPENING DISPLACEMENT TO CRACK CLOSURE STRESS FOR Al 2219-T851 [D8]

The crack tip opening displacement (CTOD) of surface microcracks, 60 to 150μm in length, developed during fully reversed fatigue loading of Al 2219-T851 was measured and compared to an average value of closure stress for the cracks. Scanning electron microscopy was used to measure CTOD at the surface tips of the cracks by using a flexurally loaded specimen in the microscope. Corresponding values of closure stress were determined by an empirical procedure, based upon measurement of two values of crack opening displacement at the crack center. The average closure stress of a microcrack was found to be largest for cracks having largest values of CTOD. For microcracks having a small average value of closure stress, the CTOD was approximately that

SC79-3372

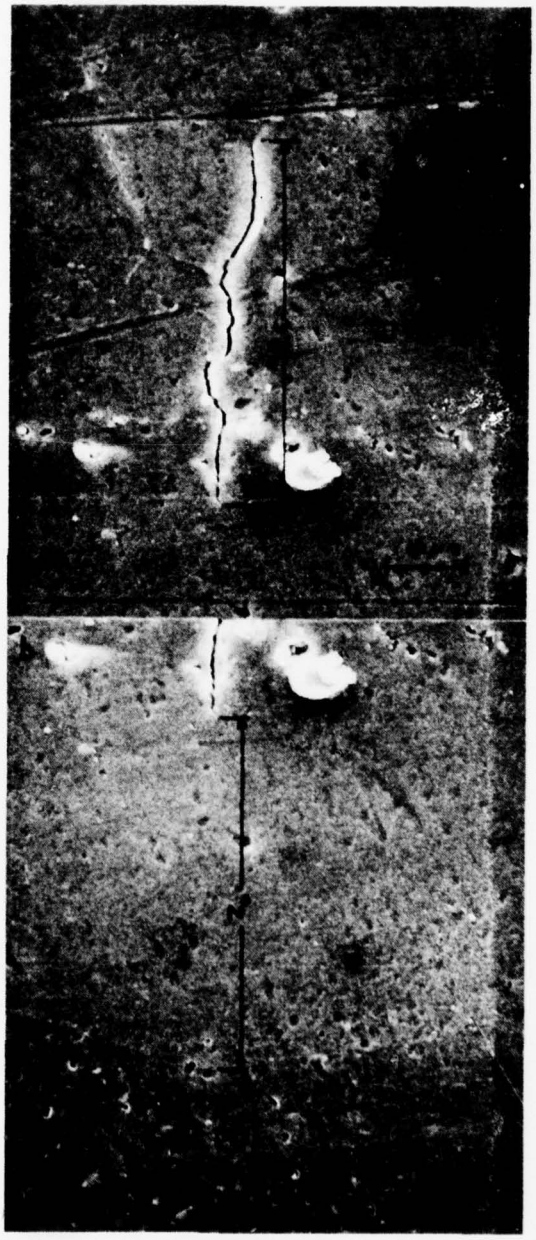

Fig. 7 Crack parameters of importance to microcrack growth.

expected from an elastic analysis of crack opening displacement by Green and Sneddon.

3.1.1 INTRODUCTION

During fatigue crack propagation, large cyclic plastic strains occur within a segment of the plastic zone just adjacent to the crack tip. The existence of this zone was predicted by Rice,[R3] and has subsequently been confirmed.[R4,5] More recently, the distribution of strain within the cyclic deformation zones of several alloys has been measured by backscatter electron channeling by Davidson and Lankford.[R6,7] Rice also noted that, on an unloading cycle, the tensile strain from the prior loading cycle was not completely reversed by compression, and resulted in crack closure at a positive value of externally applied load. As a consequence, the cyclic strain per cycle in an element of material ahead of the crack tip is reduced. Computer assisted modeling of crack closure by Newman has been based on this picture, and has successfully predicted the effect of deformation history on fatigue crack propagation rate.[R8]

Environmental factors also affect cracking rate; these have been studied by measurement of the crack closure stress, σ_{cc}.[R9-11] Environment can influence the ductility of the material at the crack tip, alter the residual tensile strain at the crack tip and, hence, change the amount of cyclic strain experienced deeper in the cyclic deformation zone where the environment may not penetrate. If the most important effect of the environment is on the cyclic strain per cycle, it is reasonable to relate the environmental effect on cracking rate to an effective intensity range, ΔK_{eff}, at the crack tip.[R12] $\Delta K_{eff} \propto (\sigma_{max}-\sigma_{cc})$, where σ_{max} is the maximum cyclic stress. In essence, ΔK_{eff} is intended to describe processes that alter only the cyclic deformation, although this is recognizably a simplification since, for instance, crack opening and closing stresses can differ.[R13] Modeling of environmental effects on crack propagation in several alloys, using ΔK_{eff}, has met with variable amounts of success. The studies are not straightforward, since measurement of σ_{cc} is still controversial [R14] and is complicated

by the fact that the closure stress can vary greatly from one location on a crack front to another.[R15]

The modeling of the microscopic aspects of fatigue crack propagation, and of crack closure will continue to improve as more is learned about the interrelationship among the magnitudes and spatial distribution of cyclic deformation near the crack tip, the effect of environment on the deformation, and the relationship of the cyclic deformation to experimentally determined values of crack closure stress. In the present work, these interrelationships are studied by using surface microcracks of the grain size developed during the fatigue of Al 2219-T851. Crack tip opening displacements (CTOD) are measured for surface cracks with lengths on the order of the grain size, and the CTOD values are compared to crack closure stresses. This is done for two values of relative humidity, for fatigue in air. Use of microcracks for the study has the advantage that large variation in closure stresses are encountered from crack to crack, which provides a wide range of values of closure and CTOD for comparison.

3.1.2 EXPERIMENTAL PROCEDURES

An Al 2219-T851 alloy, with a composition of 6.3 25% Cu, 0.3 wt% Fe, 0.2 wt% Mn, balance Al, was used for the investigation. The alloy has previously been used for crack initiation studies and its microstructure is described elsewhere.[D4] Blanks from which specimens were fabricated were taken from the center of a 2.5 cm thick plate. To minimize residual surface stress, machining cuts were made with a decreasing depth of cut per pass ending with a final cut that removed 20μm of material. The specimens were subsequently polished using a 0.05μm alumina powder. A small tapered flexural fatigue specimen design (Fig. 5) was utilized which permitted a specimen to be loaded to a desired tensile surface stress within a scanning electron microscope (SEM) for measurement of the crack tip opening displacements and closure stresses of microcracks at the surface. The specimen was loaded in the SEM by displacing the small end of the specimen a measured amount using the jig.

Test specimens were fatigued at 5 Hz in laboratory air, with either 5 or 45% relative humidity (RH), and were then transferred to the microscope for study. Loading during fatigue was fully reversed with a maximum cyclic stress, σ_{max}, of 90% of the yield strength of the alloy with σ_{yield} = 350 MN/m^2. Specimens were positioned with the surface stress axis parallel to the alloy's rolling direction. For this stress orientation, the principal crack initiation occurs at intermetallic particles located near the surface; subsequent crack propagation into the matrix is, typically, transgranular and noncrystallographic. A total of $5x10^3$ fatigue cycles were applied to each specimen in order to develop numerous microcracks on the surface with surface lengths in the range of 10 to 150μm. The longer ones of these were investigated in the present study.

A. Determination of the Average Crack Closure Stress

Conceptually, the closure stress at the tips of a microcrack at a surface can be found by measuring the crack opening displacement near the tip vs. applied surface stress. A technique of this type would be the optical equivalent of an Elber gauge.[R12] Practically, however, the displacements involved are too small for accurate measurement of the closure stresses at the tip locations. Instead, in prior research an "average" value of closure stress, $\overline{\sigma}_{cc}$, for a crack has been obtained by studying the dependence of the crack opening displacement at the center of the crack (at the surface) on applied surface stress.[D4] The closure stress thus obtained is an average in the sense that it gives a single value of closure stress for a crack, even though the actual closure stress is a function of location along the crack front. Average closure stress is defined in terms of a crack opening displacement vs. applied surface stress dependence, as illustrated in Fig. 6.

An empirical procedure for estimation of $\overline{\sigma}_{cc}$, for a surface microcrack, has also been developed;[D4-6] it requires measurement of only two values of crack opening displacement for two values of surface stress. The procedure was used in the present research and greatly reduced the work required to determine $\overline{\sigma}_{cc}$ for a given microcrack. Before the estimation

procedure is explained, the notation used to describe the crack opening displacement in later sections is described (Fig. 8).

The magnitude of crack opening displacement, of course, is a function of both location within a crack and of the applied surface stress, σ. In this paper, displacement measurements are made only at the alloy surface, as a function of location along the length of the crack. The z axis is normal to the stress axis and is, approximately, parallel to the crack path. $\delta(z,\sigma)$ is the crack opening displacement at the surface along the crack, and is measured parallel to the applied stress axis. $z = 0$ at the center of a crack. The actual closure stress, $\sigma_{cc}(\phi)$, is a function of location, ϕ, along the subsurface crack front denoted by the dashed line in Fig. 7. The surface crack tip at $z = -c$ corresponds to $\phi = 0$, and $z = +c$ to $\phi = \pi$. These are the two points on the crack front for which the crack tip opening displacement is measured. Equation (5) relates $\overline{\sigma}_{cc}$ to the displacement data.[D6] For Al 2219-T851

$$\overline{\sigma}_{cc} = 3.81\ \sigma_{max}\ \delta(0,0)/\delta(0,\sigma_{max}). \qquad (5)$$

The parameters $\delta(0,0)$ and $\delta(0,\sigma_{max})$ are the crack opening displacements at the center of the crack for a surface stress of 0 and a tensile stress of σ_{max}, respectively.

B. Measurement of the Crack Tip Opening Displacement

Measurements of the crack tip opening displacement for each crack studied were made at surface crack tips (corresponding to $z = c$ and $z = +c$ in Fig. 8) using micrographs of the crack, such as the example in Fig. 9. With the specimen loaded to σ_{max}, the crack opening displacement was measured as a function of position, z, along the length of the crack. The crack opening at each position was then normalized with respect to the maximum opening displacement that occurred at or near the center of the crack. An example of the dependence of normalized crack opening displacement along the crack length, obtained with this procedure, is shown in Fig. 10. Crack opening dis-

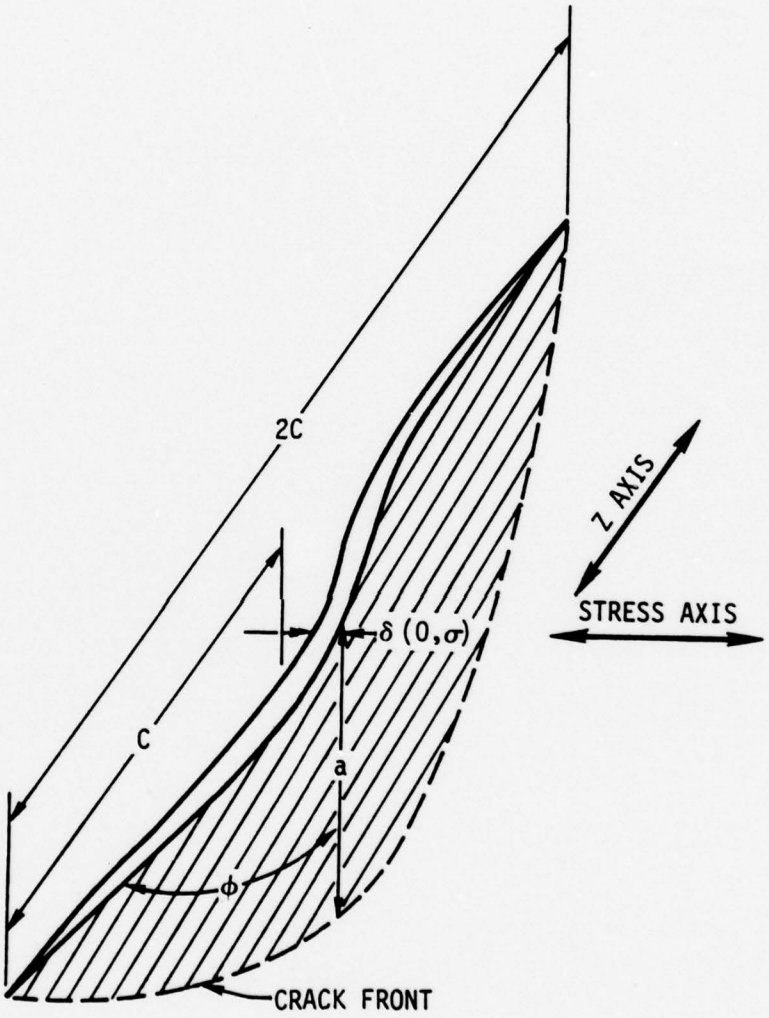

SC78-388A

Fig. 8 Perspective illustration of a surface microcrack used to define crack opening displacement measurement nomenclature.

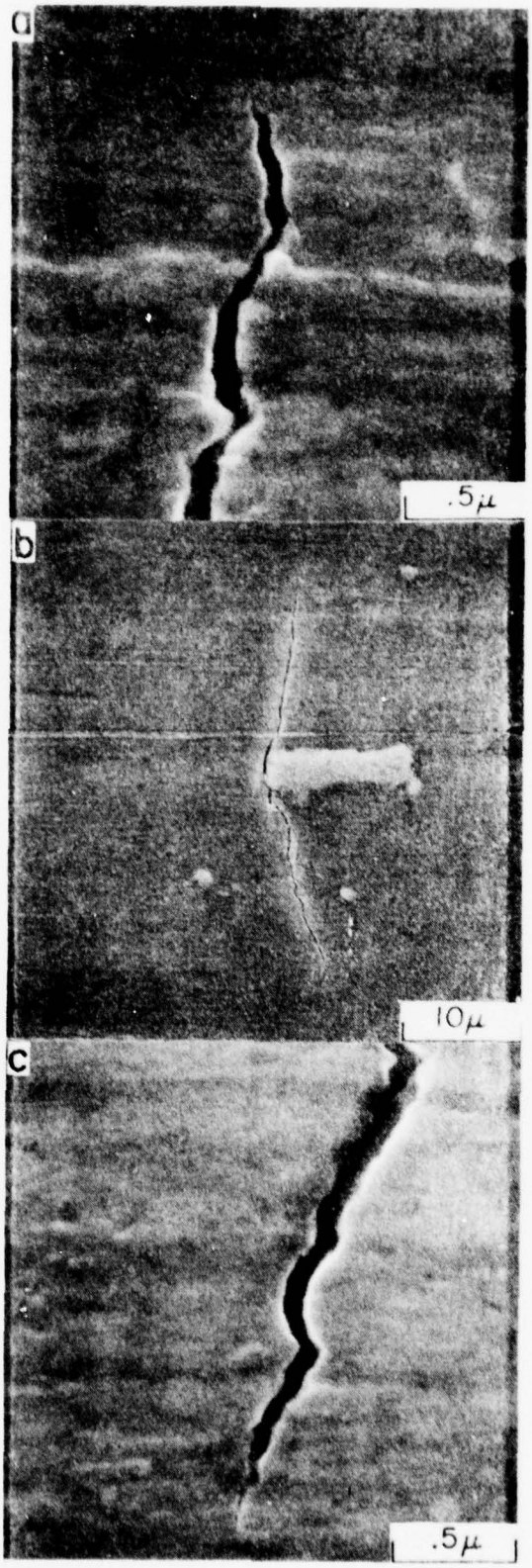

Fig. 9 Microcrack at an intermetallic nucleation site.

placement is not symmetrical to z = 0, attesting to the irregularity of the crack path and an asymmetry in crack depth.

CTOD values were obtained by extrapolating the displacement data to the two crack tips, as illustrated for one crack tip in Fig. 11. Because of the irregular structure of the crack, some ambiguity frequently existed on how far back from the crack tip to begin the extrapolation. The procedure selected to minimize this uncertainty was to look for a point within 0.5 to 3% of the total crack length from a tip for a sudden change in $d\delta(z)/dz$. An extrapolation was then made by using 3 to 4% of crack length beyond this point. The displacement $\delta(z)$ was measured parallel to the stress axis, between points on opposite sides of the fracture that could be identified as mating. An example of this technique is illustrated in Fig. 12. Opening displacement measurement must be done with some care, since chips and other artifacts in the opposing fracture surfaces can lead to an erroneous view of how the surfaces mate. One must also realize that a crack may not open precisely parallel to the applied stress axis. A suitable measurement also cannot be made if a crack tip is branched. These restrictions limit the number of cracks for which reliable CTOD measurements can be made.

Ratios of CTOD to opening displacement at z = 0 were, approximately, independent of the surface stress, provided that the surface stress was close to the average closure stress or somewhat larger. In the subsequent sections, therefore, the notations $\delta(c)/\delta(0)$ and $\delta(-c)/\delta(0)$ are used to denote the CTOD values obtained, which are normalized to the opening displacement at the crack center and taken for sufficiently large surface stress so that the ratios are essentially stress independent.

3.1.3 RESULTS

In general, the normalized CTOD values of $\delta(-c)/\delta(0)$ and $\delta(c)/\delta(0)$ obtained for the two surface tips of the same crack were not identical. As an example, Fig. 13 shows two surface tips for the same crack having substantially different values of CTOD. It was at first thought that these differences might result from the crack being especially shallow near the tip,

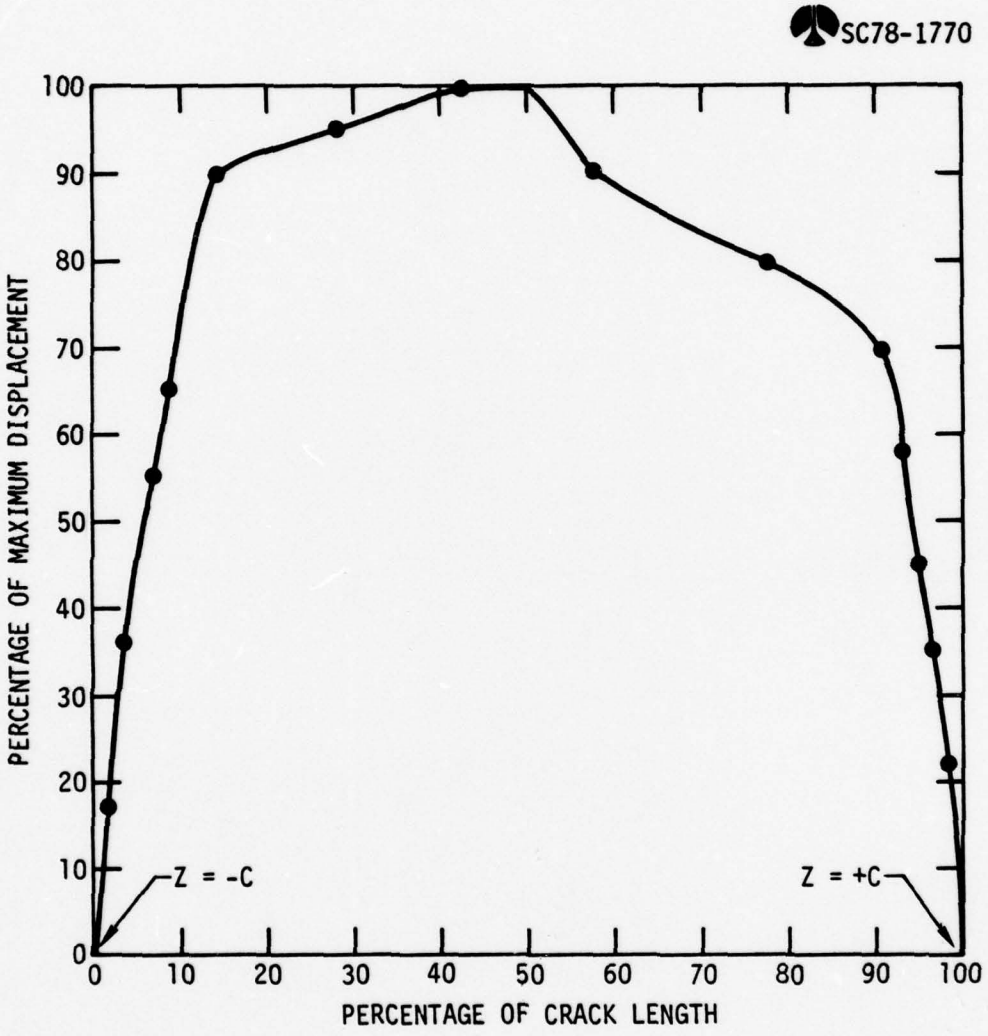

Fig. 10 Normalized crack opening displacement along the length of the microcrack.

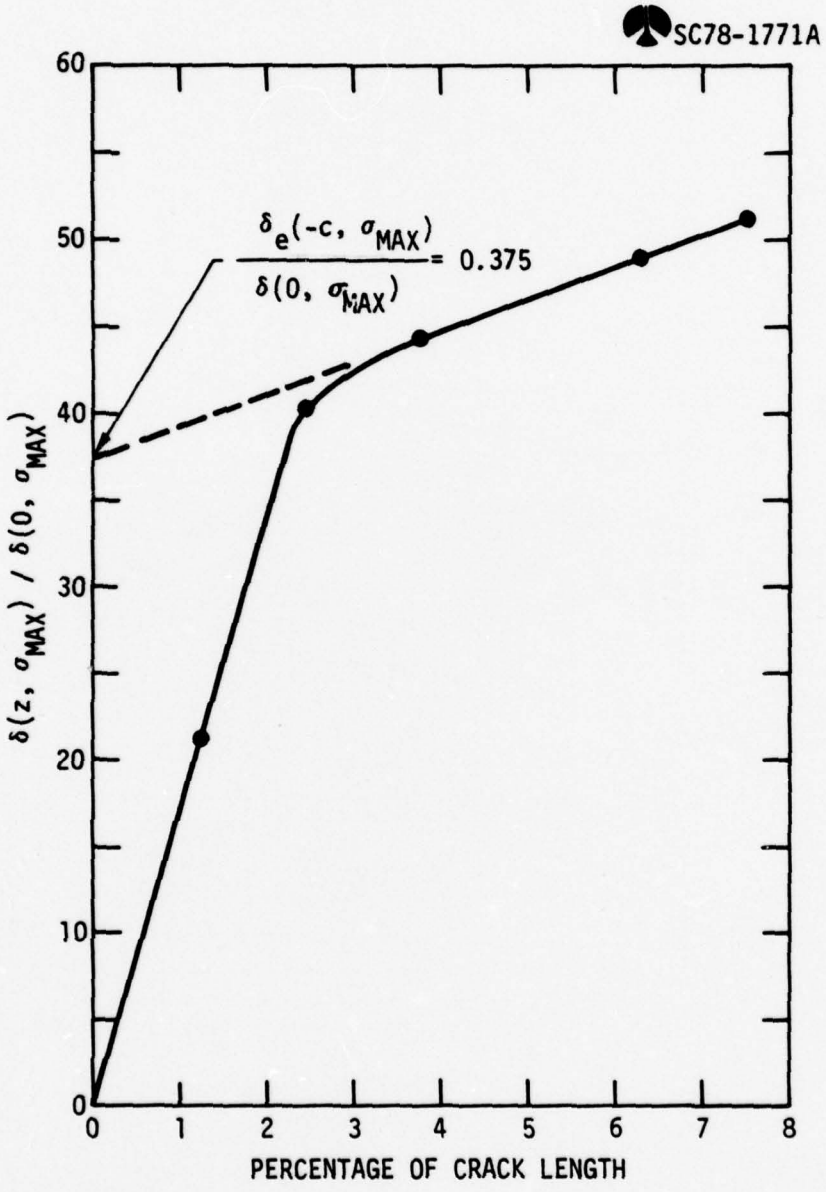

Fig. 11 Extrapolation of normalized crack opening displacement to the crack tip to determine a normalized CTOD.

SC78-3359

Fig. 12 The stress axis is parallel to arrows which indicate a set of matching features on opposing sides of the fracture surface used to measure crack opening displacement.

SC78-3360

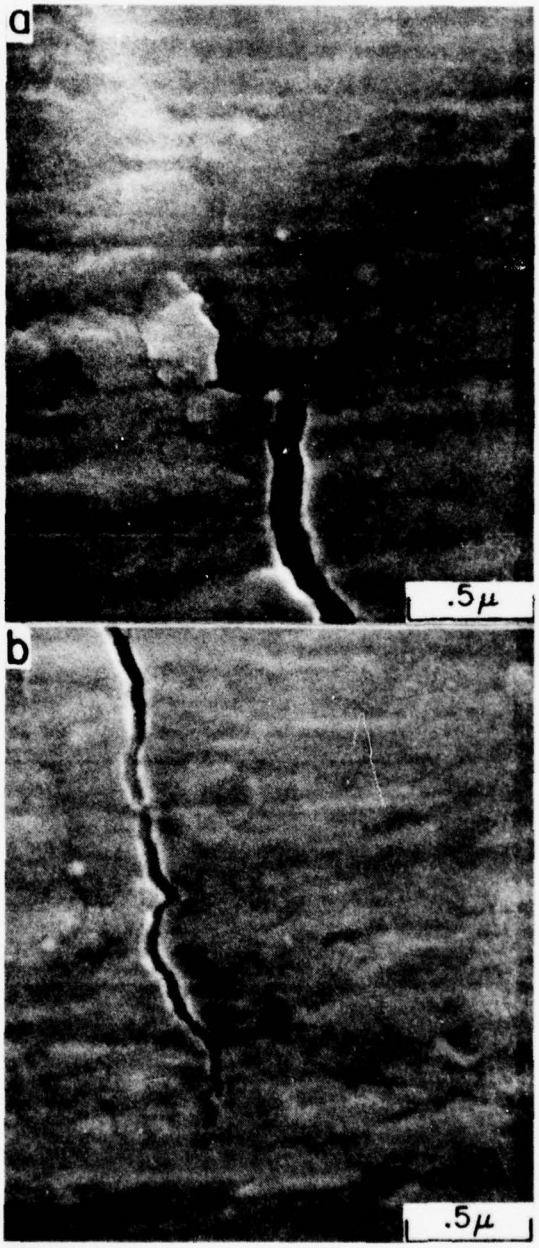

Fig. 13 Two surface crack tips of the same microcrack illustrating large variation in CTOD observed even for the same crack.

for tips with small CTOD; this, however, does not appear to be the case. The distribution in sub-surface microcrack shapes was studied by deliberately pulling fatigued specimens to failure in tension. No special crack depth variations were found which could explain the observed variation in CTOD.

A series of measurements were then done in which the values $\delta(c)/\delta(0)$, $\delta(-c)/\delta(0)$, and $\bar{\sigma}_{cc}$ were determined for a selection of surface cracks in specimens fatigued in air for either 5 or 45% RH. Relationships were then sought between the normalized CTOD values of each crack and its corresponding average closure stress. The best correlation between the average closure stress, $\bar{\sigma}_{cc}$, and the crack tip opening displacement was found in comparing the average of the two normalized CTOD measurements of a crack to $\bar{\sigma}_{cc}$. This comparison is shown in Fig. 14, where the averaged normalized CTOD is defined to be:

$$\overline{\frac{\delta(c)}{\delta(0)}} = \frac{\delta(-c)}{2\delta(0)} + \frac{\delta(c)}{2\delta(0)} \quad . \qquad (6)$$

Notice, that the figure includes data points for cracks in specimens fatigued in both 5 and 45% RH. A trend is observed for cracks with the largest value of $\delta(c)/\delta(0)$ to have the largest $\bar{\sigma}_{cc}$, and no statistically significant difference between the relationship for 5 and 45% RH is apparent. The overt effect of humidity was that at 45% RH, secondary cracking was often observed near the crack tips, such as the example shown in Fig. 15, attesting to a decreased ductility of propagation for the higher humidity. CTOD was not measured for these crack tips.

3.1.4 DISCUSSION

For the Al 2219-T851 alloy studied, fatigued with the stress axis in the rolling direction, the principle crack initiation sites are at intermetallic particles at the alloy surface (such as the example in Fig. 9). Crack closure of surface microcracks in the alloy is thought to arise from two mechanisms.[D7] Just after nucleation, when a microcrack is of a length comparable to the intermetallic from which it propagates, a misfit between

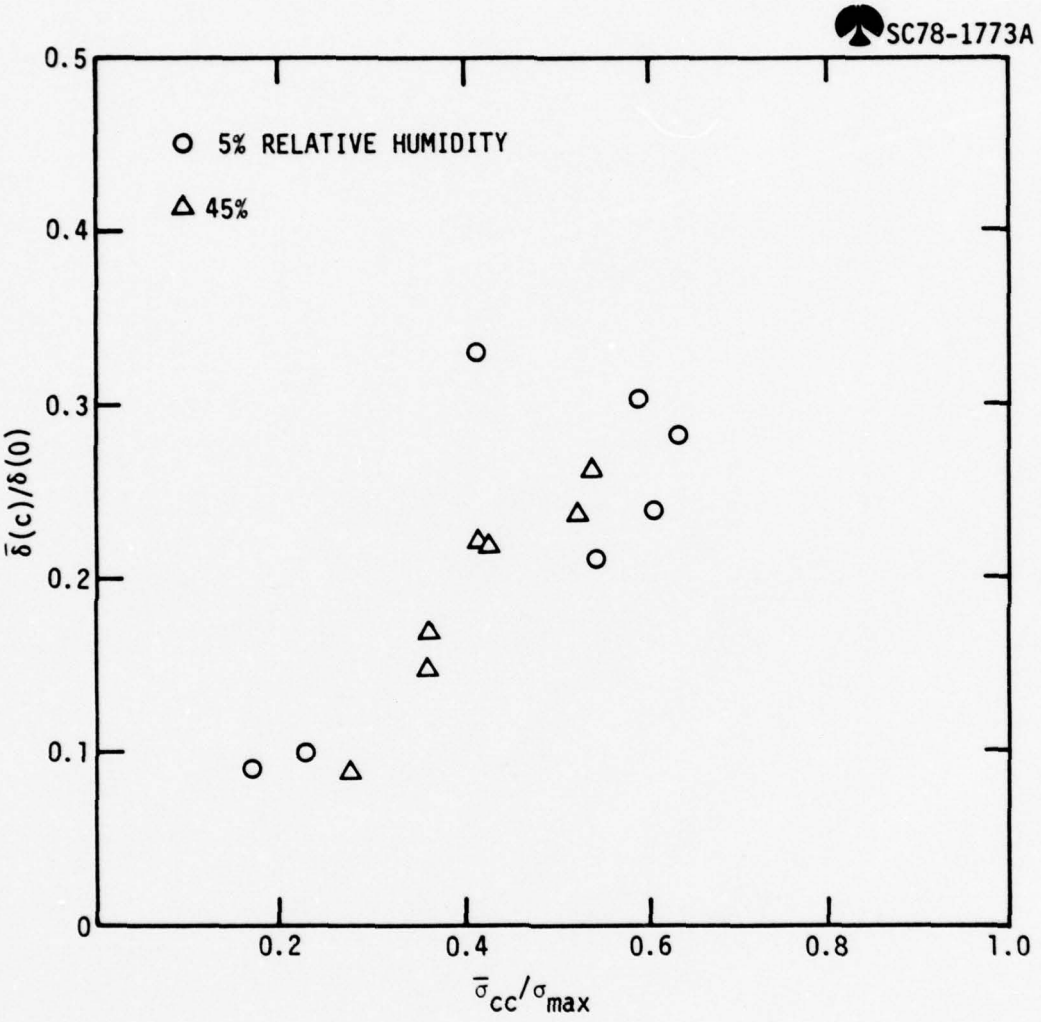

Fig. 14 Relationship of average normalized CTOD, $\bar{\delta}(c)/\delta(0)$, to average crack closure stress, $\bar{\sigma}_{cc}/\sigma_{max}$.

SC78-3361

Fig. 15 Branched crack tip at 45% relative humidity, unsuitable for measurement.

opposing fracture surfaces produces a crack closure for positive applied stress. Such misfit is of major importance only for short microcracks, and as a crack grows, the deformation behavior along the crack front becomes the factor most likely to determine closure. The present study was limited to cracks with lengths of about the width of the grains normal to the stress axis. This was done to make it more likely that crack closure resulted from residual tensile strain along the crack front. Values of $\delta(c)/\delta(0)$, found for microcracks in Al 2219-T851, range from 0.09 to 0.33 as plotted in Fig. 14. The value of 0.09 is approximately that which one would expect for the elastic opening of a crack. Some of the problems in interpretation of these observations are discussed below.

A. Elastic Limit of CTOD

The smallest values found for $\delta(c)/\delta(0)$ correspond approximately to that expected for an elastic opening of an elliptically shaped crack, a case analyzed by Green and Sneddon.[R16] This result is obtained if one approximates the surface displacement of a semi-elliptical surface crack by

$$\delta(z) = \delta(0) \left[1 - \frac{z^2}{c^2}\right]^{1/2}, \qquad (7)$$

where Eq. (7) is that obtained by Green and Sneddon along the major axis of an elliptically shaped crack loaded normal to the plane of the crack. An extrapolation procedure is then used to find the elastic CTOD, $\delta_e(c)/\delta(0)$, from the $\delta(z)$ vs. z dependence near the crack tip, as shown in Fig. 16. Naturally, there is some ambiguity as to where to begin the extrapolation. But, if the same criteria as followed with real microcracks is used, a value $\delta_e(c)/\delta(0)$ 0.09 is obtained. This is in agreement with the smallest values of $\delta(c)/\delta(0)$ found for Al 2219-T851.

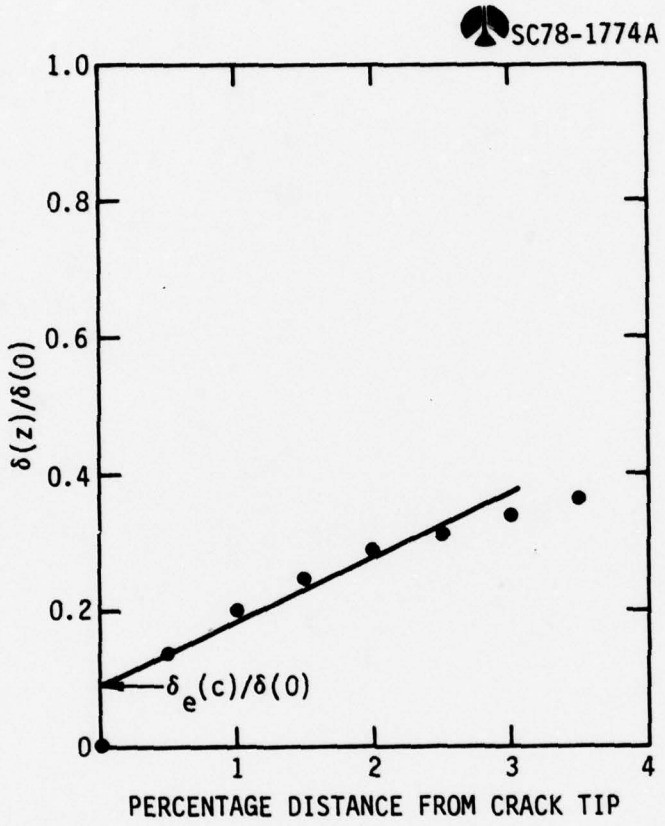

Fig. 16 Extrapolation of Eq. (7) to determine an elastic CTOD.

B. Plastic Deformation Limit on CTOD

Rice [R3] has suggested that the maximum crack tip opening displacement $\delta(c,\sigma_{max})$ should approximately be

$$\delta(c,\sigma_{max}) = \frac{\varepsilon_y}{2} R_p \ , \qquad (8)$$

for cyclic loading, where ε_y is the strain at the yield strength and R_p is the diameter of the plastic zone. For the range in CTOD values encountered in the present work, the corresponding calculated values of R_p extend from 35 to 130μm. In contrast, the plastic zone diameter, calculated using the polycrystalline yield strength for a 60μm long surface crack at 0.9 σ_{yield}, is 24μm. The crack tip opening displacements and associated apparent size of zone of deformation at the crack tip are, therefore, larger than expected from the continuum theory. As inferred from Eqn. (8) however, the range in plastic zone sizes is approximately the same as the range in the width of the grains in the alloy in the direction of crack propagation.

Recent refinements of Eq. (8) by McKeeking [R17] to incorporate the effect of strain hardening on CTOD provides corrections much too small, although in the right direction, to explain the large values of CTOD observed. The form of Eq. (8) is not convenient for evaluation of the CTOD for small R_p, since the CTOD value predicted does not converge to the elastic CTOD. If the elastic evaluation is taken as a lower bound, and R_p from Eq. (8) as an upper bound, the observations of this study are consistent with a range in R_p values from 0 to 130 μm.

C. Further Considerations

The relationship between CTOD and closure stress, found for microcracks of the grain size, is substantially different from results previously reported for macrocracks in fracture mechanics specimens. Langford and Davidson [R8] for instance, have observed, a decreasing CTOD at maximum stress as a crack was propagated into a zone producing increased closure. Some years

ago, Adams [R19] pointed out that this variation should be expected if residual tensile strain in the wake of the crack was responsible for the crack closure phenomenon. In contrast, for cracks of the grain size, the trend found here is for closure stress to increase with increased CTOD. Previous studies of the closure phenomena have found other ways in which the behavior of microcracks differs from that for macrocracks. Some of the prior observations for microcracks were that:

1. $\delta(z = 0) \propto \sigma$, for $\sigma > \overline{\sigma}_{cc}$; whereas from continuum theory $\delta(z = 0)$ is expected to be noticeably nonlinearly related to stress.[D7]

2. $\overline{\sigma}_{cc} \propto \sigma_{max}$; where from continuum theory $\overline{\sigma}_{cc} \propto \sigma^2_{max}$ is expected.[D7]

3. $\overline{\sigma}_{cc}$ can be estimated from the geometry of the crack path as seen from the surface, and cracks differing in size, but not shape, tend to have the same closure stress.[D4]

4. Tensile spike overloading increases $\overline{\sigma}_{cc}$ in proportion to the magnitude of the overload, with no measureable crack propagation.[D7]

To this list can be added the latest results:

5. $\overline{\sigma}_{cc}$ increases as the average normalized CTOD of the surface crack tips increase.

6. For cracks with small closure stress, the average normalized CTOD of the surface tips is approximately what would be observed if there were no plastic deformation at the crack tips.

7. The large values of CTOD observed for some of the microcracks are substantially larger than expected from continuum theory, and plastic zone sizes estimated for these are approximately the size of the largest grains in the material.

An analytic theory to describe these observations remains to be advanced. Qualitatively, however, substantial consistency between the observations is achieved if it is assumed that the size of the plastic zone (or at least the zone of significant deformation) at a surface tip of a microcrack is approximately the distance of the crack tip to the nearest grain boundary, and that the zone size is consequently independent of the applied stress. One can only speculate as to how this circumstance might arise, but the factors unique to the microcracks, studied here, are: the plastic zone size expected from continuum theory is on the order of the grain size; because of the small crack size, the plane stress condition at the surface crack tips dominates the deformation behavior; and achieving even a comparatively small stress intensity entails application of a large surface stress to a specimen.

To explain the closure observations for microcracks accumulated in this and in prior work, the following model is suggested. Except for special circumstances where fracture surface roughness leads to closure, the inflection in the crack opening displacement vs applied surface stress dependence, interpreted as closure for microcracks, is not the result of a physical closure of the crack in the wake of the crack front. Instead, the departure from elastic behavior on unloading is the result of a cessation of reverse yielding in the plastic zone. (As a parenthetical note, it should still be useful to describe crack propagation in terms of ΔK_{eff} for this case. The so-called "crack closure" has the same effect of reducing the cyclic deformation per cycle experienced by material at the crack tip.) The crack opening displacement-applied stress dependence typically observed is approximately linearly elastic for $\sigma > \bar{\sigma}_{cc}$, because the size of the plastic zone is independent of the applied stress. One also expects from this that the CTOD $\propto \sigma$ for $\bar{\sigma} > \sigma_{cc}$ leading to a closure stress that is proportional

to σ_{max}, as is observed. Humidity reduces the ductility of the alloy in the grain sized plastic zone, leading to lower CTOD, a smaller $\bar{\sigma}_{cc}$, and, hence, to accelerated crack propagation rates. Rapid variation in crack propagation rate, as a microcrack grows, are principally the result of changing closure stress along the crack front as the crack position changes relative to the grain boundaries. This picture is, of course, more complicated if crack branching occurs. A dimensionally based argument can be made that

$$\frac{\sigma_{cc}}{\sigma_{max}} \propto \frac{z_o}{2c} \quad , \tag{9}$$

where z_o is the distance of a surface crack tip to the closest grain boundary in the direction of crack propagation, and 2c is the crack length.

Naturally, there is a substantial amount of speculation in the model and further investigation is required to test it. Two opportunities in this regard are: (1) compare dc/dN to ΔK_{eff}, by measuring the microcrack closure stress using the CTOD relationship of Fig. 14, and (2) look for a relationship between CTOD and the distance of microcrack tips to neighboring grain boundaries. Development of an analytic model of the deformation properties of cracks with plastic zones of fixed size is also ultimately essential for complete interpretation of the observations of these studies.

An additional coment is required. It might be expected that if $\delta(c)/\delta(0) = 0.09$, then $\sigma_{cc} = 0$. Values of $\sigma_{cc} = 0.2$ are more typical, as per Fig. 14. It is suggested that crack closure due to misfit of the opposing fracture surfaces (i.e., fracture surface roughness) places a lower bound on σ_{cc}. The presumption is that the mechanism which gives the largest closure stress at a point on a crack front which determines the closure stress at that point. A value of 0.2 for $\bar{\sigma}_{cc}$ is in the range commonly found for closure stresses in 2000 series aluminum alloys for large cracks in fracture mechanics specimens.

3.1.5 SUMMARY

Crack tip opening displacement (CTOD) measurements were made for surface microcracks with lengths of aproximately the grain size developed during the fatigue of Al 2219-T851. Correlations were sought between the two CTOD values obtained for each crack for the surface crack tips, and the average closure stress of the crack. Average closure stress was obtained by using empirical relationship based on two measurements of the crack opening displacement at the crack center -- one at zero and the other at maximum applied surface stress. The average closure stress, $\bar{\sigma}_{cc}$, is an average in the sense that a single closure stress value is obtained by the measurement procedure, even though it is expected that the actual closure stress varies with location along the crack front. Cracks with the largest values of CTOD exhibited the largest values of $\bar{\sigma}_{cc}$. This trend was strongest when a comparison was made between $\bar{\sigma}_{cc}$ and the average of the two CTOD values obtained for a crack, with CTOD normalized to the opening in the crack center. A model was proposed to explain these and prior results for microcracks, results which differ substantially from closure observations for large cracks in fracture mechanics specimens. The key element of the model is the suggestion that for microcracks, the plastic zone size (or at least the zone of significant deformation) at the surface is approximately given by distance between crack tip and the grain boundary toward which a crack is propagating. Furthermore, it is noted that if the closure stress at the surface tip is proportional to the plastic zone size, much of the closure observations unique to microcracks are qualitatively explained. An immediate application of the model is to permit an experimental comparison between the rate of propagation of surface microcracks during fatigue, and an effective stress intensity range, ΔK_{eff}. The closure stress values needed to complete the calculations of ΔK_{eff} can be obtained by CTOD measurements.

3.2 CRACK CLOSURE STRESS EFFECTS ON THE RATE OF PROPAGATION OF SURFACE MICROCRACKS DURING THE FATIGUE OF Al 2219-T851 [D9]

The rate of propagation of surface microcracks of approximately 25-100 μm in length, developed during fatigue loading of Al 2219-T851, has been measured and compared to predicted cracking rates using an effective stress intensity range, ΔK_{eff}, analysis. Crack closure stress and crack shape factor parameters needed to evaluate ΔK_{eff} for individual crack tips were obtained from measurement of crack tip opening displacement and crack compliance, respectively. Although the ΔK_{eff} description of microcrack growth is recognizably simple, it indicates that crack closure contributes significantly the rate of early propagation of microcracks in the alloy.

3.2.1 INTRODUCTION

As a result of fatigue, unusually large postive crack closure stresses are developed by surface cracks of lengths comparable to the grain size in aluminum alloys.[D3-6] While a trend towards reduced rate of propagation of such microcracks with increased closure has been noted, a quantitative comparison between measured closure stress and cracking rate remains to be made. As with prior exeriments for crack closure propagation in fracture mechanics specimens, it is desirable to determine an effective stress intensity range, ΔK_{eff}, to describe the cracking process. ΔK_{eff} is defined to be proportional to the cyclic stress range experienced at the crack tip (i.e. to $(\sigma_{max}-\sigma_{cc})$, or the maximum cyclic stress minus the crack closure stress).[R12] A problem heretofore in evaluating ΔK_{eff} for microcracks is that σ_{cc} is a function of location along the crack front. Crack closure values previously obtained for microcracks have been averages, termed $\overline{\sigma}_{cc}$ hereafter, obtained from compliance measurements made at the center of surface microcracks.[D4] Such a measurement determines a single value of "closure stress" for a crack (this is the sense in which "average" is meant) and hence suffices only for the study of <u>trends</u> in closure stress development with crack propagation.

Recently, a correlation has been found for Al 2219-T851, between the crack tip opening displacement (CTOD) of a microcrack tip and σ_{cc}, with σ_{cc} increasing with increasing CTOD.[D8] In the present research ΔK_{eff} values at surface microcrack tips in Al 2219-T851 are obtained with closure stresses estimated by measuring CTOD. It has been suggested that observed variations in σ_{cc} and CTOD as a microcrack propagates, reflects changing constraints on the plastic zone size, or at least the zone of significant deformation, with distance between the microcrack front and grain boundaries.[D8] The crack shape factor (depth/ length) needed to complete the determination of ΔK_{eff} is found by measurement of the compliance of the microcrack. Using these techniques, the rate of crack propagation of microcracks developed during fatigue in Al 2219-T851 is compared to ΔK_{eff}, as the local closure stresses change with crack propagation.

3.2.2 EXPERIMENTAL PROCEDURE

The Al 2219-T851 alloy used for the investigation had a composition of 6.3 wt% Cu, 0.3 wt% Mn, 0.3 wt% Fe, balance Al. Miniature flexural fatigue specimens were machined from the center of a 2.5 cm thick rolled plate. To reduce residual surface stress, the cutting depth during final machining was decreased with each pass, ending with 20μm of material removed per cut. Finally, specimens were polished with a 0.05μm alumina powder. Results reported here were obtained using a flexural fatigue specimen geometry and a loading jig (Fig. 5) designed for use in a scanning electron microscope (SEM). The specimen geometry utilized provides a uniform tensile stress over the specimen surface, whose magnitude is determined by measurement of displacement of the specimen end. Loading of the specimen in the microscope is required for measurement of the microcrack tip opening displacements.

Each test specimen was fatigued (R = -1) at 5 Hz in air at room temperature, and at a relative humidity of 40%, with $\sigma_{max} = 0.9\ \sigma_{yield}$. Surface stress calibration in the specimen gauge section was obtained by strain gauges. The absolute stress accuracy is estimated to be ±5%, the relative accuracy from one cracking area to another in on the order of ±1%. Material

orientation was with the rolling direction parallel to the principle stress axis. For this orientation, the alloy yield stress was 350 MN/m^2 and the crack nucleation was at intermetallic particles at or near the surface, followed by transgranular crack propagation.

Microcrack propagation data were taken as follows: A specimen was given 2.5×10^3 fatigue cycles in air and was then transferred to the SEM. Microcracks were located, each having a surface length of approximately 25μm. These were microcracks for which propagation into the matrix was already well established.

High resolution micrographs were taken, along the length of each crack studied, with the specimen under load: a) concentrating particularly on the two crack tips for use in estimation of the crack tip closure stress from CTOD; and b) around the center of the crack for use in estimating both closure stress and the crack shape factor. With these measurements completed, the specimen was returned to the air environment for additional fatigue. The sequence of cracking parameter measurements and fatigue was repeated in the same manner in increments of 500 cycles until 5×10^3 cycles had been applied. At this point, the cracks being observed were approximately 100μm long. The resulting data are used to compare measured crack propagation rate, dc/dN, and ΔK_{eff}. Before discussion of these results, it is advantageous to briefly describe the calibration procedures utilized in estimating the crack tip closure stresses and crack shape factor.

A. CTOD Estimate of Crack Tip Closure Stress

An empirical relationship has previously been noted between the crack tip opening displacement determined under load and crack closure stress for microcracks developed by the fatigue of Al 2219-T851.[D8] While theoretical arguments can be advanced for the form of a general relationship between closure stress and CTOD, the functional relationship between these quantities has been demonstrated for an R = -1, $\sigma_{max} = 0.9\ \sigma_{yield}$ test condition. In the current experiment, specimens were fatigued for this same condition.

The nomenclature used to describe the crack opening displacement along a microcrack is illustrated by Fig. 8. $\delta(z,\sigma)$ is the opening at point z along the crack length, at surface stress σ, and is measured parallel to the applied stress axes. Mating features on opposite sides of the crack opening are identified and used to define the crack opening. $\delta(c,\sigma)$ is the CTOD and is obtained by extrapolation of $\delta(z,\sigma)$ to z = c.

Equation (10) is used to estimate the closure stress at a crack tip from the CTOD.[Taken from Fig. 14.]

$$\sigma_{cc}/\sigma_{max} = 2.1\ \delta(c,\sigma)/\delta(0,\sigma). \qquad (10)$$

A requirement on the validity of Eqn. (10) is that σ exceed $\bar{\sigma}_{cc}$. Therefore, it is most convenient to use $\sigma = \sigma_{max}$. The quantity $\delta(0,\sigma)$ is the opening, for the same σ, at the crack center. It should also be recognized that *Eqn. (10) is an empirical* description of microcrack closure stress spanning two different mechanisms of closure for microcracks: 1) closure due to fracture surface roughness of importance for $\sigma_{cc} \sim 0.2\ \sigma_{max}$; and 2) closure due to residual tensile strain at the crack tip, important for $\sigma_{cc} > 0.2\ \sigma_{max}$. When the tensile residual at a crack tip is small $\delta(c,\sigma)/\delta(o,\sigma) \sim 0.1$, corresponding to the elastic limit of CTOD. In this case, surface roughness leads to a closure stress of $\sim 0.2\ \sigma_{max}$ for Al 2219-T851.

B. Crack Shape Factor Calibration

To complete the calculation of ΔK_{eff}, it was necessary to determine approximately, the subsurface shape of an observed microcrack as well as the manner in which the shape changed with increment in propagation. It is expected from an analysis by Green and Sneddon [R16] that the quantity $\delta(0, \sigma_{max})/2c$ will approximately be a constant for a given shape factor, a/2c. An experimental calibration was performed, as follows, to relate the two quantities. A specimen of Al 2219-T851 containing surface cracks induced by fatigue was pulled in tension to failure. Numerous microcracking thumbnails were exposed from which the distribution of shape factors was

measured. One such crack is shown in Fig. 17. There tends to be some distortion in the apparent shape of the crack due to tearing in the region of the crack tips near the surface. Consequently, the crack shape was measured using markers of crack front location within the fracture surface, such as at the arrow. The distribution in observed crack shapes as a function of crack length is shown in Fig. 18.

A relationship between a/2c and $\delta(0, \sigma_{max})/2c$ was obtained by comparing Fig. 18 to a plot of the scatter in $\delta(0, \sigma_{max})/2c$ with 2c obtained for Al 2219-T851 in prior research.[D5] The mean value of a/2c observed was approximately 0.362 and led to a linear correction to a/2c for variation in $\delta(0, \sigma_{max})/2c$ given by Eqn. (11).

$$\frac{a}{2c} = 0.362 + 25.1 \left[\frac{\delta(0,\sigma_{max})}{2c} - 1.5\times10^{-2} \right] . \qquad (11)$$

While, owing to the comparatively small variation in crack shapes around the mean, it might have sufficed to use the mean in calculating ΔK_{eff} for all microcracks, use of Eqn. (11) was found to decrease the apparent data scatter in comparison of dc/dN to ΔK_{eff}.

3.2.3 RESULTS

The requirement for accurate measurement of CTOD substantially limits the number of cracks suitable for study. A key element is that one must be able to identify a number of matching features on opposite sides of the crack, for definition of $\delta(z,\sigma)$ near the crack tip. While numerous cracks were observed, data shown here are limited to four selected cracks for which reliable $\delta(z,\sigma)$ values were obtained for a major portion of the crack propagation. Crack #1 (Fig. 19) is included because it had the largest observed range in dc/dN. In the later stage of fatigue, the lower crack tip of crack #1 branched in passage of an intermetallic particle (Fig. 20). This reduces the accuracy of the calculated ΔK_{eff} for that tip for the 4.5×10^3 and 5×10^3

SC79-3379

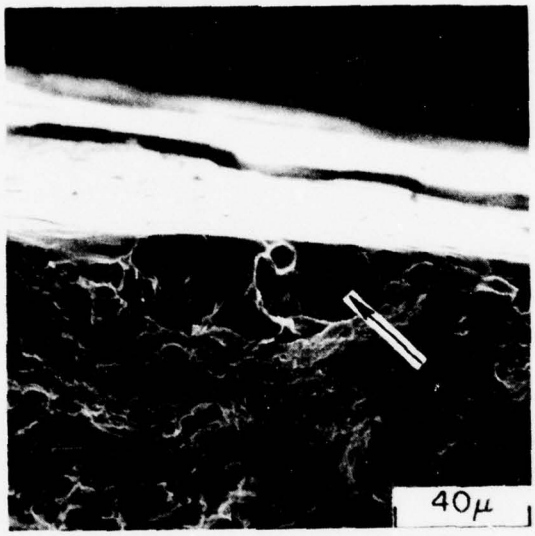

Fig. 17 Fatigue crack thumbnail used to measure crack shape factor using marker line such as at arrow.

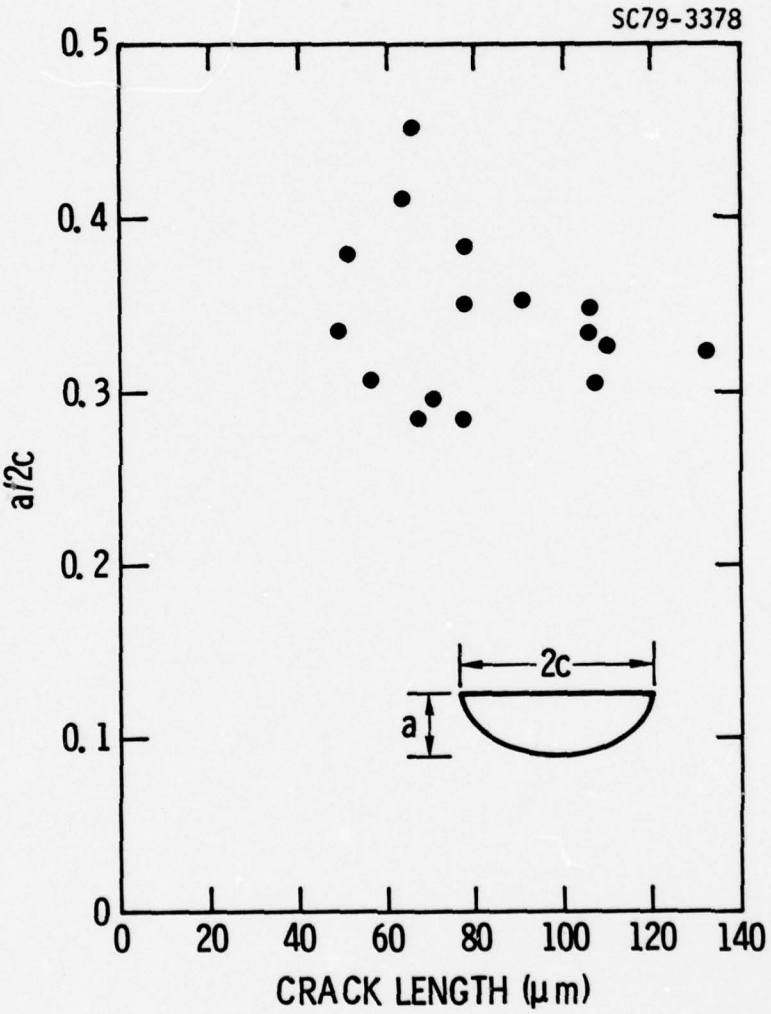

Fig. 18 Trend in crack shape factor with microcrack length.

SC79-3377

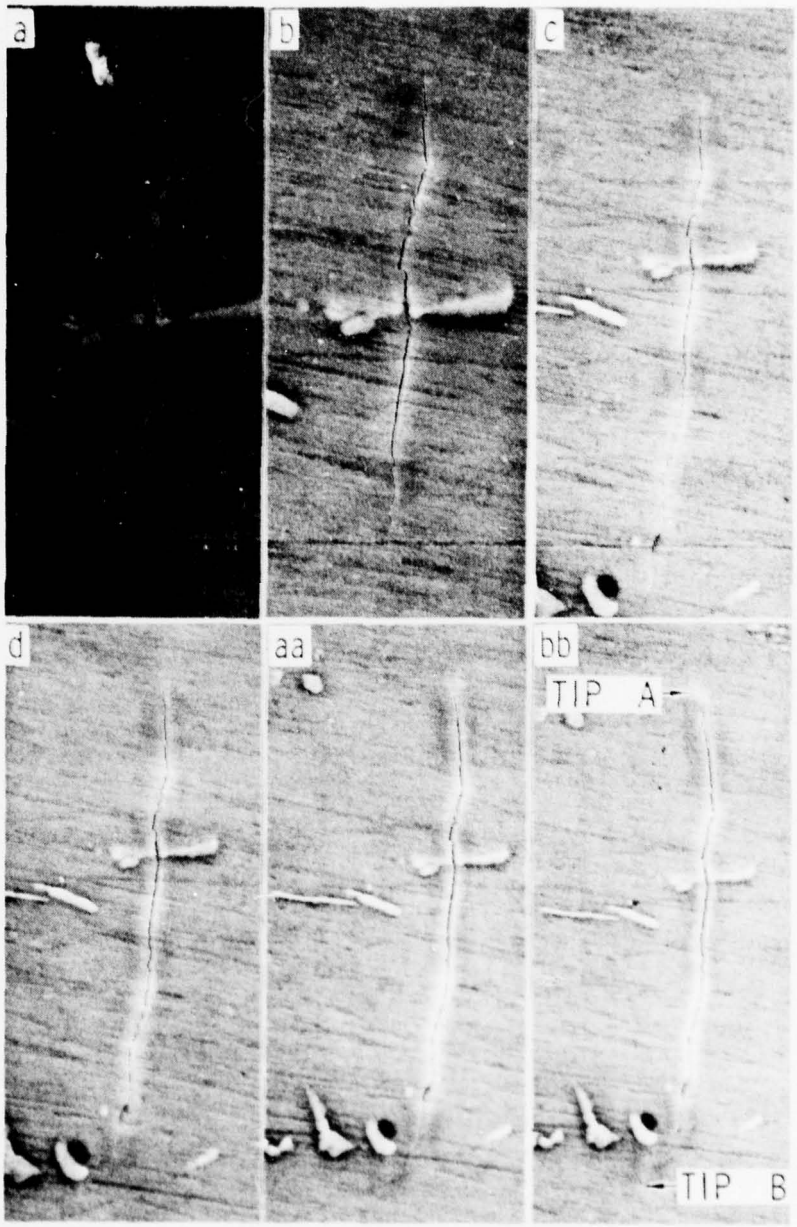

Fig. 19 Microcrack #1 for 500 cycle increments in fatigue cycles from 2.5×10^3 to 5.0×10^3 cycles. Crack length at (a) is 30μm, at (b) is 88μm.

SC79-3376

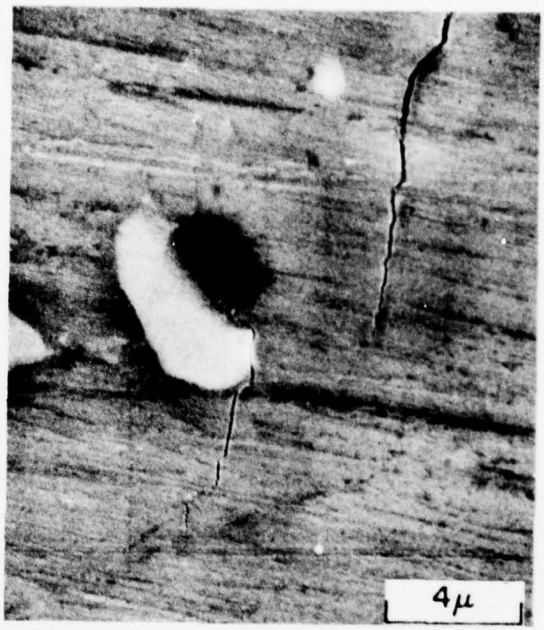

Fig. 20 Branching of crack tip B (crack #1) in passage of an intermetallic.

fatigue cycle increments. The upper tip of crack #1 is referred to as Tip A and the lower tip as Tip B. The average rate of propagation of each tip of #1 with fatigue is given in Fig. 21. Figure 22 shows, as a function of fatigue, the estimated closure stress for tips A and B of crack #1 and Fig. 23 the crack shape factor. The σ_{cc} values and a/2c were obtained using the procedures previously described. Averages of the values of the parameters were calculated between two successive fatigue increments to generate the data plotted.

The utility of a Paris equation corrected for crack closure [R12] to describe microcrack propagation is accessed.

$$\frac{dc}{dN} = A\,[\Delta K_{eff}]^m \quad , \tag{12}$$

where

$$\Delta K_{eff} = (\sigma_{max}-\sigma_{cc})\sqrt{a}/Q\ F(a/c,\phi) \quad . \tag{13}$$

A and m are material constants. Q is a correction for plastic zone size, which is itself dependent upon the crack shape factor. Using the notation of Smith and Sorenson,[R20] the parameter $F(a/c,\phi)$ is used to describe the variation in stress intensity range along the crack front. The case of interest here is $\phi = 90°$, corresponds to propagation along the surface. Values for $F(a/c, \phi = 90°)$ vs a/c were obtained for use in the present calculation by extrapolating to shallow crack depth values for F obtained by Smith and Sorenson. Thus, the approximation has been made that the cracks are semi-elliptical, planar, normal to the applied stress and are unaffected by the presence of intermetallic particles such as near tip B of crack #1.

Predicted to measured dc/dN values for crack #1 are compared in Fig. 24. Here, a value of m = 2 has been assumed, typical of that encountered for Al alloys for macrocrack propagation corrected for closure. The dotted line is the value of dc/dN which would correspond to a $\sigma_{cc} = 0$ case. In Fig. 25, dc/dN is compared to ΔK_{eff} for the four test cracks studied, from which a best linear regression fit of m = 1.6 is obtained. Figure 25 is taken from additional analysis of the microcrack propagation data supported by Rockwell IR&D funds.

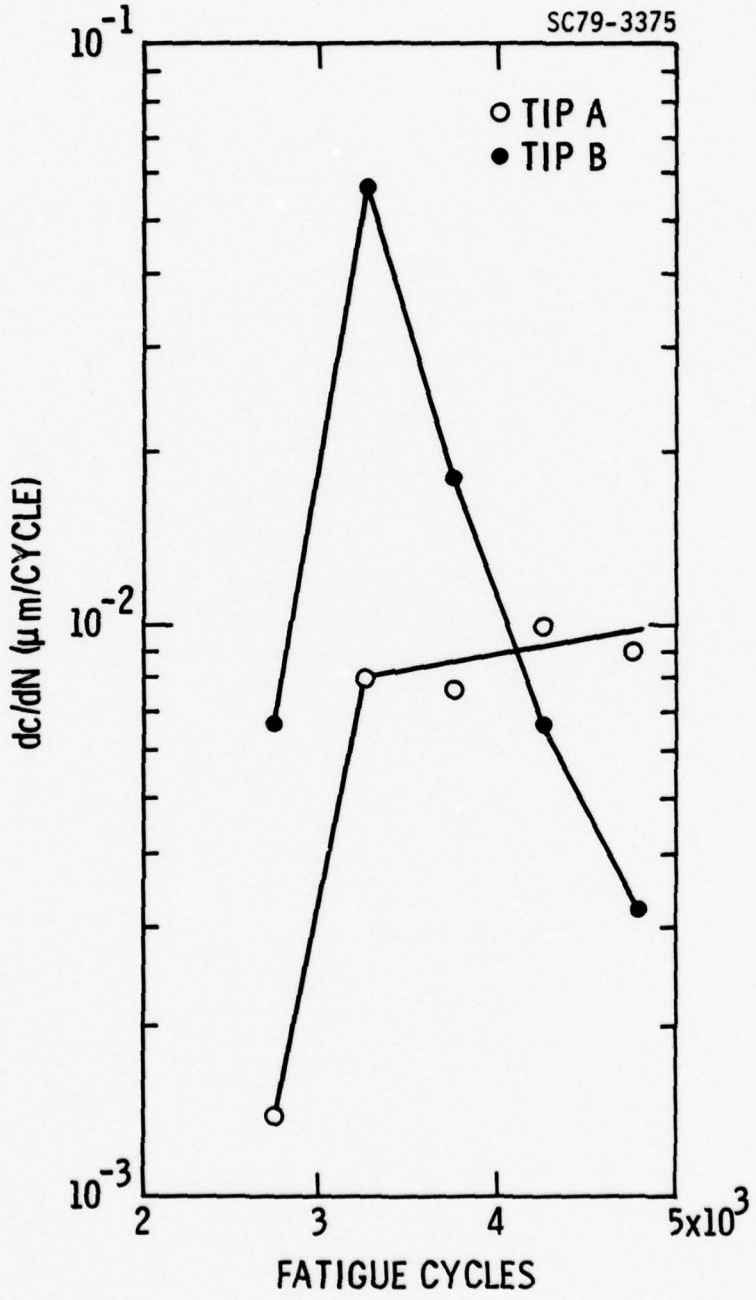

Fig. 21 Measured rate of propagation of the two tips of crack #1.

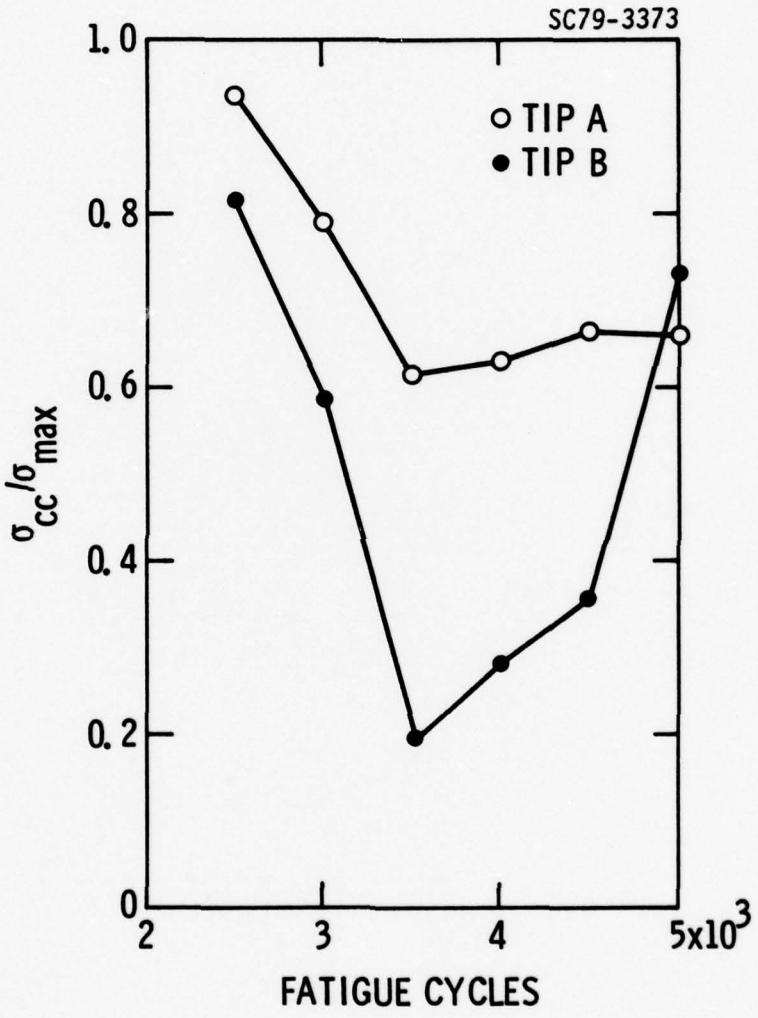

Fig. 22 Crack tip closure stresses estimated from CTOD.

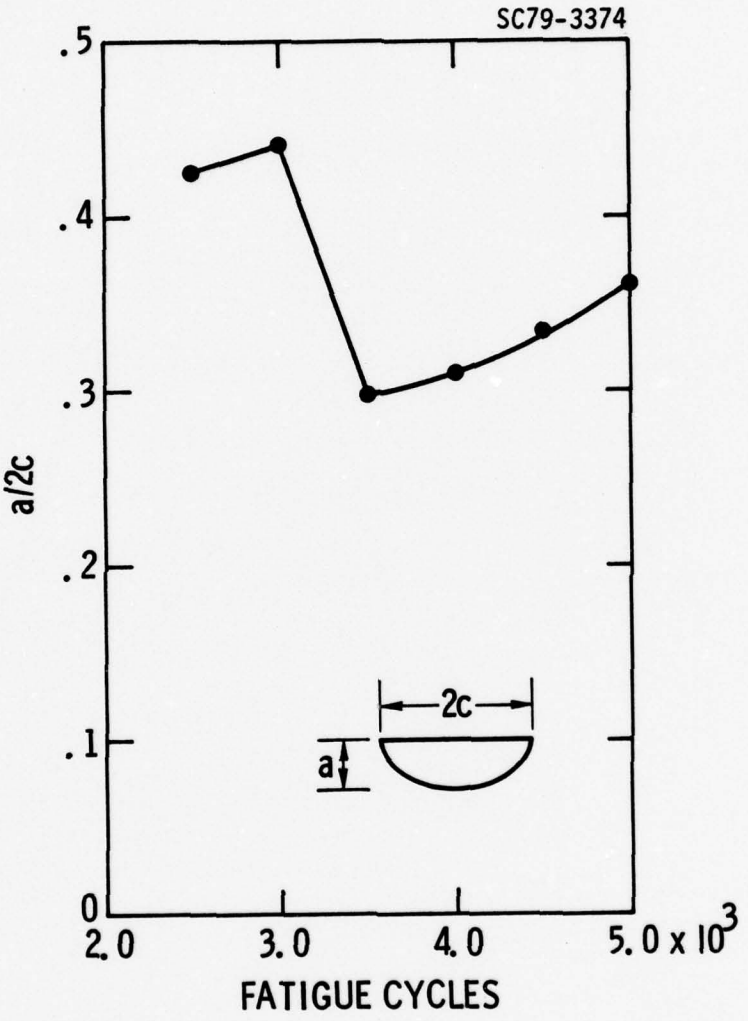

Fig. 23 Crack shape factor estimated from crack compliance.

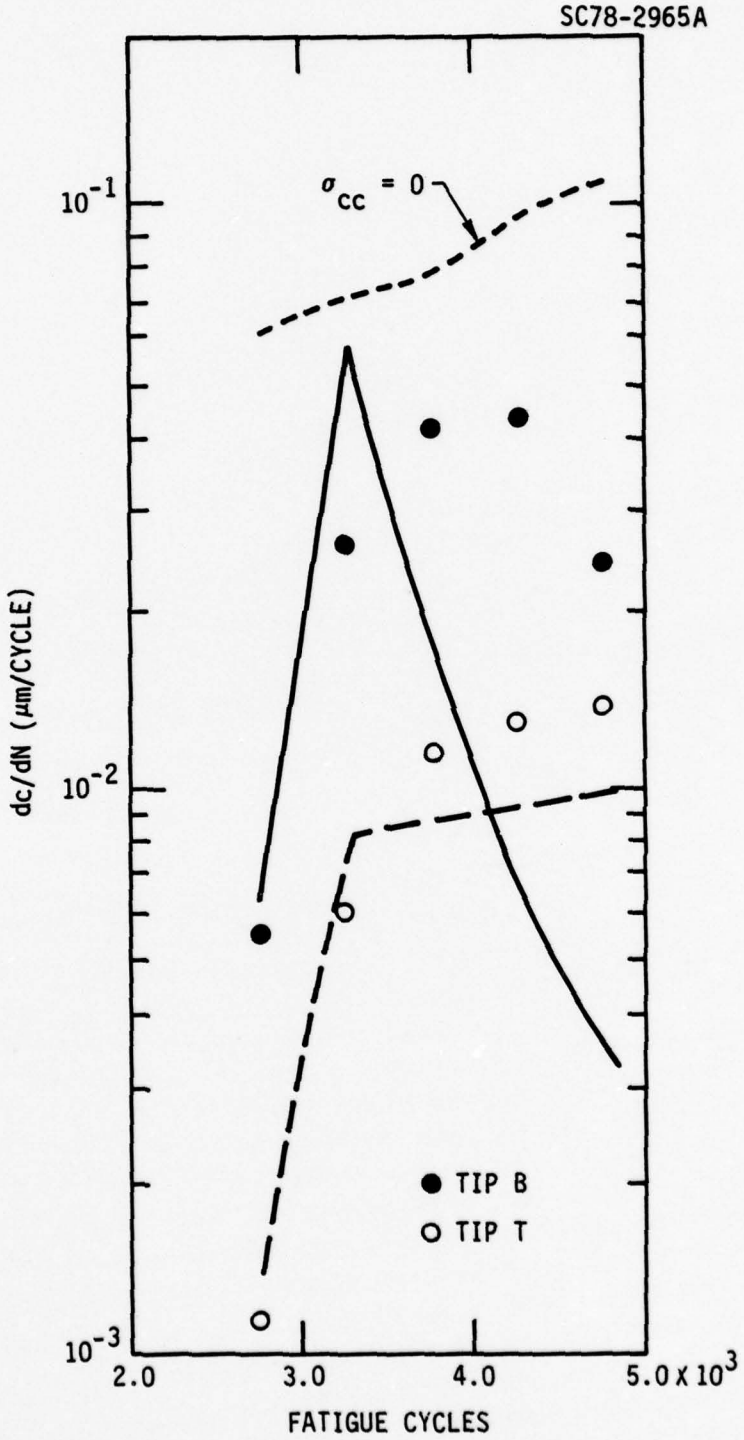

Fig. 24 Comparison of predicted to measured cracking rate for crack #1. Dots are the predicted values. Uppermost curve is predicted cracking rate in the absence of crack closure.

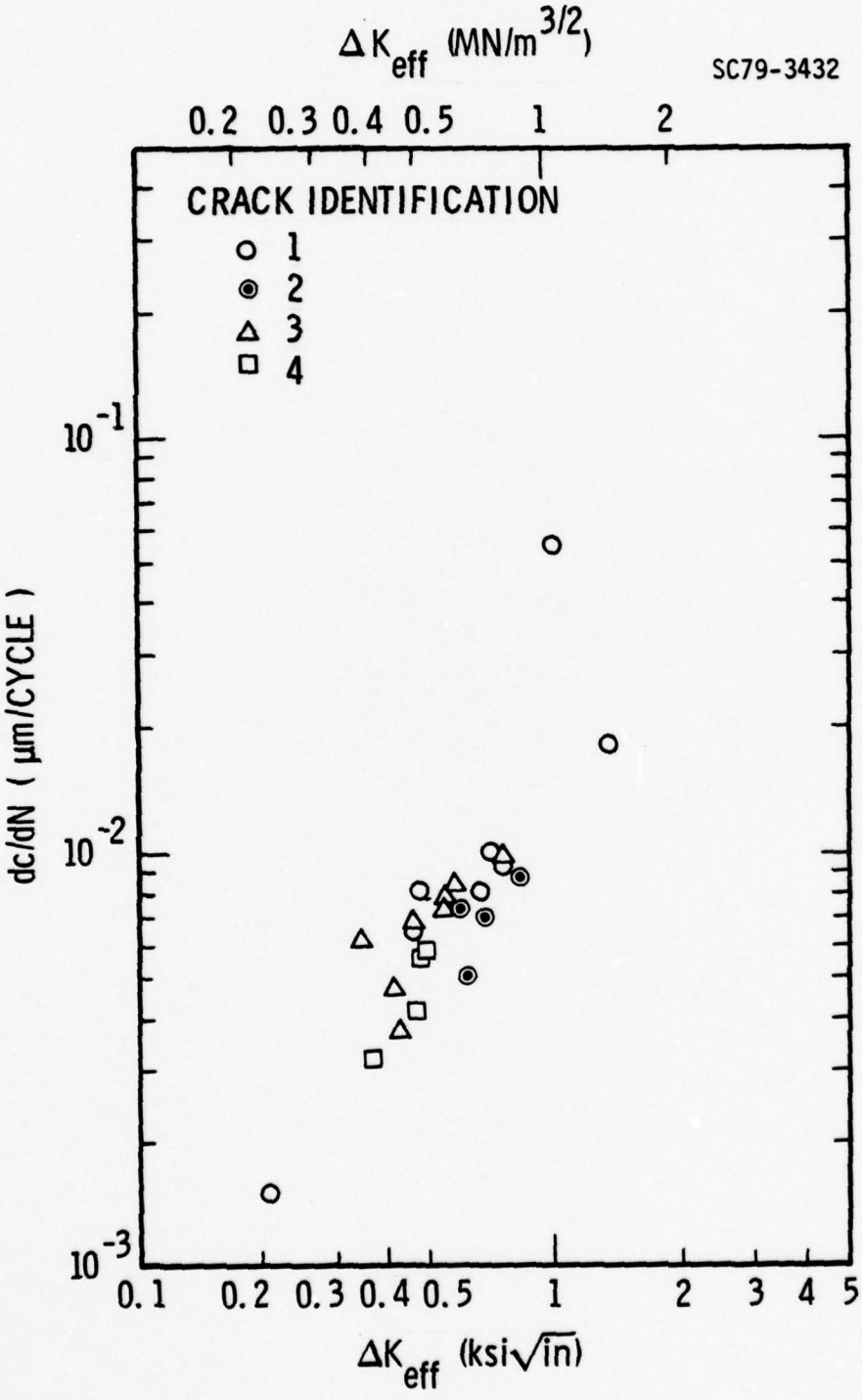

Fig. 25 Comparison of microcrack propagation rate to ΔK_{eff}.

3.2.4 DISCUSSION

From experience with macrocrack propagation in fracture mechanics specimens, one generally associates a large cyclic range in CTOD during loading with a correspondingly large range in stress intensity and consequently with large crack propagation ranges.[R7,18] This model requires modification for microcracks because the plastic zone size is not determined by continuum mechanics, but instead is, approximately, given by the size of the grain at the crack tip.[D8] With a large grain at the tip, a large CTOD can be achieved with a small applied stress intensity. The accumulated damage is smaller per cycle, compared to an analogous large CTOD in a fracture mechanics specimen, because the strain from which the CTOD develops is distributed over a proportionally larger volume.

To appreciate the success of the ΔK_{eff} analysis, it must be recognized that there is no meaningful correlation between dc/dN and ΔK (uncorrected for closure). Present data are taken very near the threshold stress intensity range value for propagation, with $\Delta K < 2$ MN/m$^{3/2}$. Crack closure stress is therefore a major factor in determining the rate of propagation of surface microcracks in Al 2219-T851. The simple ΔK_{eff} analysis also provides an empirical means to predict the cracking rate for individual microcracks, because the closure stress can be estimated from the size of the grain at a crack tip.[D8]

Although it is useful in this case, the ΔK_{eff} description of microcrack propagation is a simplification on reality. It is almost certain that the cessation of reverse yielding in the plastic zone, on unloading, is a function of location in the zone for a given external stress - not the sharp transition which the present model assumes. Further analytic insight is necessary for special problems applicable to regime where microstructure constrains deformation. It is probable that computer modeling of closure processes for microcracks would be highly useful in development of an improved effective stress intensity range description of the early propagation of microcracks.

3.2.5 SUMMARY

Microcrack propagation rates are measured using scanning electron microscopy for surface microcracks developed in Al 2219-T851 by fully reversed loading cyclic fatigue. Propagation is followed for selected cracks in the range of 25 to 100μm in surface length. At increments in the fatigue lifetime, the closure stress at individual microcrack tips, at the surface, is estimated from a measurement of the crack opening displacement at the tip. Crack shape factor is estimated from a measurement of microcrack compliance for the same fatigue increments. The closure and crack shape data are used to calculate an effective stress intensity range, ΔK_{eff}, for comparison to measured microcrack propagation rates. The results indicates that closure stress is a major factor in determining the rate of propagation of surface microcracks in Al 2219-T851.

3.3 THE RELATIONSHIP OF CRACK TIP OPENING DISPLACEMENT TO GRAIN SIZE FOR MICROCRACKS IN Al 2219-T851 [D10]

Departures between theoretical and experimental values of plastic zone size have recently been reported for low values of stress intensity in fracture mechanics specimens.[R18] The differences are attributed to a failure of the continuum theory. A related effect has also been observed for surface microcracks with lengths of approximately the grain size in Al 2219-T851.[D7,8] In this instance, analysis of microcrack tip opening displacement (CTOD) measurements led to the suggestion that the zone of significant plastic deformation, for the special case of microscopic cracks, is determined by the size of a grain at the surface crack tip. This observation is of particular interest because, potentially, it leads to a method to predict the effect of grain size on the rate of growth of microcracks during fatigue. It has been previously shown that the magnitude of crack closure resulting from residual tensile deformation at a microcrack tip can be determined by measuring CTOD.[D8] Furthermore, an effective stress intensity range, ΔK_{eff}, calculated by using such closure values, has led to adequate prediction of rates of microcrack growth in Al 2219-T851.[D9]

In the experiments described here, correlations were sought between CTOD and the distance of the crack tip to the grain boundary for surface microcracks in Al 2219-T851. Flexural fatigue specimens of an alloy with composition 6.3 wt% Cu, 0.3% Fe, 0.2% Mn, balance aluminum were prepared for minimum residual surface stress by machining with sequentially reduced cutting depths. The specimens were polished with a 0.05μm Al_2O_3 powder and then given a light chemical etch to permit identification of the grain boundaries. A triangular shaped constant surface stress specimen design was used, miniaturized to permit insertion into a scanning electron microscope (SEM).[D4] Loading of a specimen to a desired tensile surface stress in the microscope was accomplished using a jig, described elsewhere,[D4] which displaced the end of the specimen a measured amount. Specimens were fatigued in air, for either 5 or 60% relative humidity (RH), with the principal stress axis in the rolling direction (for which $\sigma_{yield} = 350\ MN/m^2$), and then transferred to the microscope for study. During fatigue, the loading was fully reversed with a peak cyclic stress, σ_{max}, of 0.9 σ_{yield}. Approximately 2500 fatigue cycles were applied to each specimen to achieve a distribution of microcrack sizes on the surface.

Figures 7 and 8 are used to define the crack measurement nomenclature employed here. The crack length, 2c, is measured at the surface from tip to tip. The distance of a crack tip to the next grain boundary, called z_o, is measured along the z axis, which is normal to the stress axis. The origin of the z axis is placed at the center of the crack at the surface. σ is the surface stress and the CTOD measurements were made for $\sigma \sim \sigma_{max}$. To reduce additional complexity which might arise in interpretation of how to measure z_o with variable grain shape, measurements were restricted to grains elongated in the rolling direction, with crack propagation normal to the rolling direction. Crack opening displacement as a function of location along a crack is represented by $\delta(0,\sigma)$ and was measured parallel to the applied stress. Two crack opening displacement values were found for each crack tip studied; 1) An opening displacement at the crack center termed $\delta(0,\sigma)$; 2) and at the crack tip termed, $\delta(c,\sigma)$. $\delta(c,\sigma)$ was obtained by extrapolation of $\delta(z,\sigma)$ near

the tip, to z = c. $\delta(c,\sigma)/\delta(0,\sigma)$ has previously been related to the closure stress, σ_{cc}, at a microcrack tip.

The ratios $\delta(c,\sigma)/\delta(0,\sigma)$ and $z_0/2c$ are compared for the two test humidities in Figs. 26 and 27. z_0 is normalized to the microcrack length because it is known that the crack closure stress is independent of crack length for a given surface trace of the cracking path.[D4] Each data point is from an individual microcrack tip of a crack for which $30<2c<150\mu m$. $\delta(c,\sigma)/\delta(0,\sigma)$ is interpreted as a measure of tensile strain at the crack tip. The minimum value of $\delta(c,\sigma)/\delta(0,\sigma) \sim 0.1$ and corresponds to the expected elastic limit of CTOD.[R16] Thus, it is found that $\delta(c,\sigma)/\delta(0,\sigma)$ increases linearly with $z_0/2c$ with approximately no plastic deformation for $z_0 = 0$. A shallower slope for the 60% RH data is attributed to a reduced ductility of the material at the crack tip as a result of alteration by humidity. Indeed, the slope of the $\delta(c,\sigma)/\delta(0,\sigma)$ vs. $z_0/2c$ line can be interpreted as a measurement of the local ductility of the aluminum matrix in the microscopic region at the crack tip.

Also of interest is to use the data of Figs. 26 and 27 to relate the closure stress at the crack tip to $z_0/2c$; where crack closure is used in a generic sense to refer to all processes leading to a reduced cyclic plastic deformation per cycle at the crack tip, and hence to $\Delta K_{eff} \propto (\sigma_{max}-\sigma_{cc})$, the maximum cyclic stress minus the closure stress. For surface microcracks in aluminum alloys, σ_{cc} can arise from two independent mechanisms: (a) physical contact of opposing fracture surfaces; (b) as a result of residual tensile strain at the crack tip. Unlike the mechanism (a), often observed on macrocracks in fracture mechanics specimens, mechanism (b) is not typically found to lead to physical contact behind the crack tip at σ_{cc}. Instead, "closure" at a positive external load on unloading is interpreted as resulting from a cessation of reverse yielding in the plastic zone. Mechanism (a) is of special importance in the very early stage of microcrack growth, just as a crack leaves an intermetallic particle from which it has nucleated, in which case, σ_{cc} can approach σ_{max}. For grain sized cracks, surface roughness also places a lower limit on the closure stress of $\sigma_{cc} \sim 0.2$ for Al 2219-T851. It

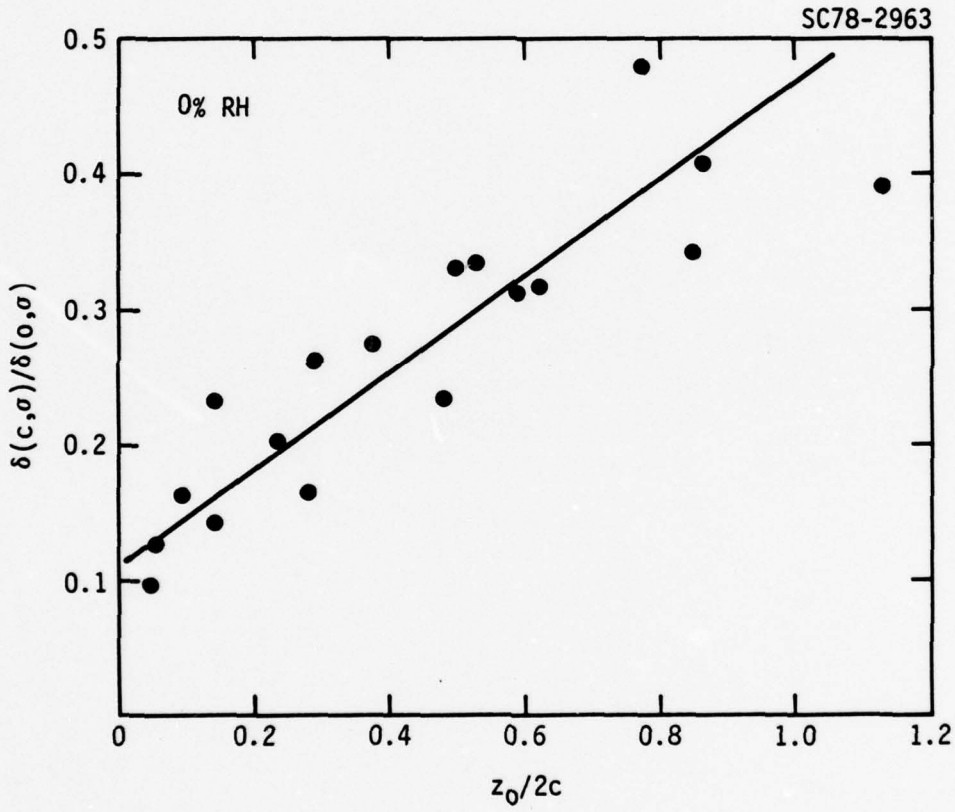

Fig. 26 Relationship of CTOD to distance of crack tip to grain boundary for 5% RH.

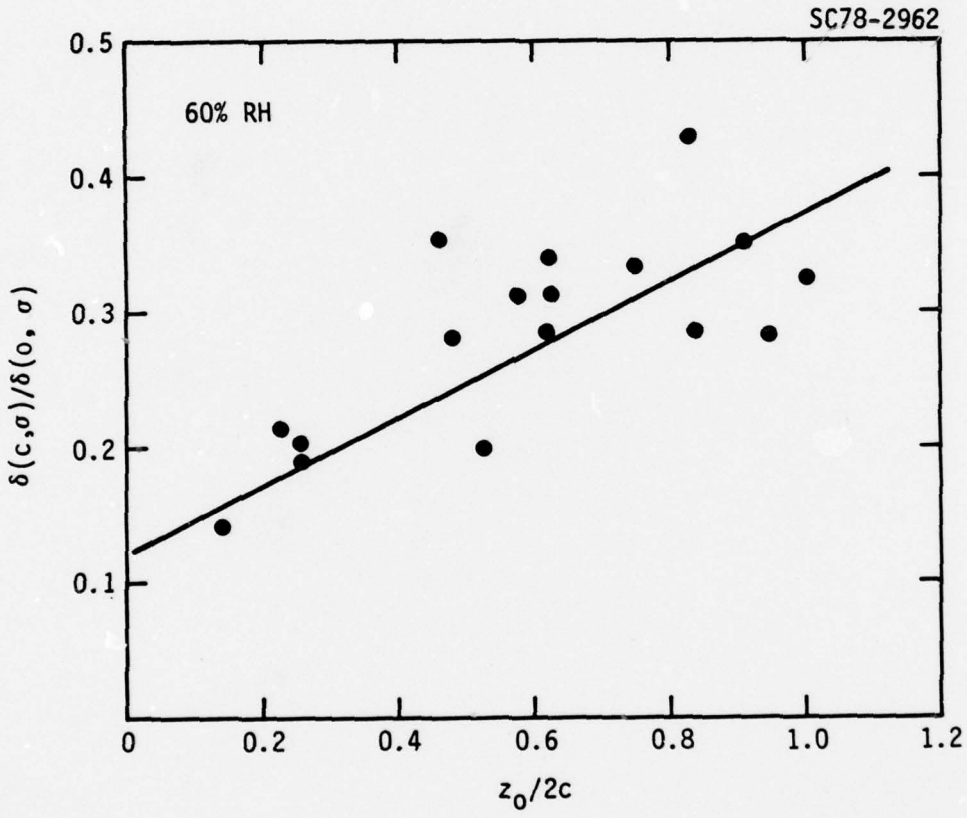

Fig. 27 Relationship of CTOD to distance of crack tip to grain boundary for 60% RH.

is the mechanism giving rise to the largest σ_{cc} at a point on a microcrack front which determines σ_{cc} at that point.

Prior comparison of $\delta(c,\sigma)/\delta(0,\sigma)$ to σ_{cc} [Fig. 14] (instead of $z_o/2c$) has found a trend similar to that reported in Figs. 26 and 27, differing only in behavior for small $\delta(c,\sigma)/\delta(0,\sigma)$. CTOD measures only the effect of tensile residual at the crack tip on closure and if $\delta(c,\sigma)/\delta(0,\sigma)$ is small, σ_{cc} is determined by surface roughness. To obtain a relationship between σ_{cc} and $z_o/2c$, we ignore data for $\sigma_{cc} \sim 0.2$ in the $\delta(c,\sigma)/\delta(0,\sigma)$ vs σ_{cc} measurement. This leads to

$$\frac{\sigma_{cc}}{\sigma_{max}} = 1.2 \frac{z_o}{2c} , \tag{14}$$

for 5% RH, and

$$\frac{\sigma_{cc}}{\sigma_{max}} = 0.8 \frac{z_o}{2c} , \tag{15}$$

for 60% RH. The relationships describe only the effect of residual tensile strain at the crack tip on the closure stress, and larger values of σ_{cc} from roughness may supercede that given by the relationships in special circumstances. Additionally, the data from Figs. 26 and 27 were obtained for cracks which had propagated beyond the grain of nucleation. Within the grain of nucleation, crystallographic cracking tends to decrease the closure stress, and it is found that (14) and (15) define upper bounds of the observed closure stress in that case. For sufficiently long crack length, one also expects the plastic zone size to revert to that given by a continuum analysis for the material studied. The crack size at which this occurs is presently known only approximately ($\simeq$ 400 μm), corresponding to an average of four grain diameters in the alloy investigated. As a final comment, it is of particular interest that measurement of z_o at the surface suffices to determine trends in closure stress. Undoubtly, scatter in the data in Figs. 26 and 27 relate in part to the crystallographic orientation of individual grains and to subsurface grain

shape. However, it is suggested, that slip parallel to the surface is easier owing the lack of a bulk constraint, leading to a CTOD, and hence closure stress, more sensitive to the surface section dimension of the grains than would otherwise be observed.

4.0 FATIGUE BEHAVIOR PREDICTIONS

Models of nucleation and early crack growth have been used to develop a computer (Monte Carlo) simulation of fatigue failure. While the simulation is restricted to failure arising from crack nucleation at surface particles we believe the techniques discussed can, in the future, be generalized to describe much more complex failure processes. Crack coalescence remains to be the least understood of the three sequential elements of failure and will require substantial amounts of further investigation. Presently, coalescence enters the simulation only from the statistics of location of the microcracks. We have observed that for cracks of no more than a few grain diameters in length, the surface tips of neighboring cracks do not sense each others' presence until the tips are in a common grain. This can be expected from the nature of the deformation described for single microcrack growth. Once in a common grain, however, changes in crack tip closure stress are complex and remain to be described. We make some simplifying assumptions about the nature of the coalescence process once crack tips are in a common grain.

Because of the success of the ONR supported research, Rockwell International is continuing support of the lifetime modeling along the lines first identified in the ONR effort. In addition to the modeling experiments the ONR funding was used to develop the one-dimensional simulation of fatigue failure described in Section 4.1. The experimental data against which the predictions are tested were obtained with Rockwell support. Subsequent to the completion of the ONR effort, a more general two-dimensional model of nucleation has been developed and we discuss this briefly to illustrate potentials for research in this area in the future. Section 4.1 is comprised of comparison of predicted to measured fatigue behavior on a microscopic level and therein is described the general simulation approach. In Section 4.2 further details of the crack coalescence simulation are provided along with predictions of alloy and humidity effects on scatter and mean values of fatigue lifetime.

4.1 A MONTE CARLO SIMULATION OF MICROCRACK GROWTH

A Monte Carlo based computer simulation of the fatigue crack initiation phase of an aluminum alloy is described. Processes modeled include 1) nucleation of microcracks at intermetallic sites at the alloy surface; and 2) early microcrack propagation wherein cracking rate is retarded, and highly sensitive to the alloy microstructure in the region of a microcrack. The simulation is used to predict the distribution in closure stress values for surface microcracks as a function of crack length and the number of fatigue cycles. Predicted and measured distributions in closure stress values are compared using Al 7075-T7 alloys for two different grain sizes.

4.1.1 INTRODUCTION

Analytical models of nucleation and early growth of microcracks on the surface of aluminum alloys subjected to fatigue loading have recently been proposed and evaluated.[D2,8-10] The models are simplistic and yet contain sufficient reality to make reasonable predictions of the rates of crack formation and propagation in the initiation stage of the fatigue failure process. We describe here an extension of this research, in which the microscopic failure process models are used to develop a Monte Carlo simulation of fatigue failure of certain aluminum alloys. The general approach is to nucleate cracks in simulation, which then propagate according to rules relating cracking rate to the location of the surface microcracks relative to neighboring grains. In more advanced versions of the simulation, crack coalescence is allowed. Specimen fatigue lifetime is determined by the smallest number of fatigue cycles required for any crack present on a specimen to reach a critical size. Scatter in fatigue lifetime from (simulated) specimen to specimen then results from statistical fluctuations in alloy microstructure consistent with the average alloy microstructure.

An alternate form of such a simulation is to predict distributions in microcrack parameters with fatigue. This can include numbers of cracks, distribution in crack size, and parameters of importance to remaining lifetime prediction - such as distribution in crack closure stress with microcrack

length. Such microscopic predictions have several applications including: (a) definition of fatigue damage at intermediate stages of failure - for use in analyzing nondestructive evaluation techniques to determine remaining fatigue lifetime, (b) to provide simulated microcrack parameters for comparison to measured parameters. It is this latter use that is of interest here, as it provides a means to determine the strengths and weaknesses of the models on which the simulation is based.

Specifically, we discuss a comparison between predicted and measured values of the average closure stress of surface microcracks, as a function of crack length, for two Al 7075 T7 alloys. Crack closure is a prime factor in determining the rate of propagation of the surface microcracks during fatigue. An important mechanism of closure stress development is from residual tensile strain at the microcrack tip.[D8] It has previously been shown that when this mechanism pertains, the magnitude of the closure stress is sensitive to the size of the grains ahead of the propagating microcrack.[D10] Consequently, the simulated versus experimental comparisons are made for two alloys having different mean grain sizes, in the direction of crack propagation (75 μm and 25 μm).

While we do not report on predicted fatigue lifetime in the present section the general form of the simulation, used with respect to lifetime prediction, is described, as the microscopic predictions discussed were extracted as a by-product of the simulation. The simulation technique described is an early version of a program which has subsequently been revised to reflect further mechanistic insights and to incorporate additional sophistication in approximations required in the representation of reality. Limitations and approximations in the simulation, used to generate the predictions, are discussed as well as opportunities and approaches for improvement of the simulation.

4.1.2 THE FATIGUE MODEL

We begin by describing the sequence of fatigue failure events to be modeled and the general approach used to simulate fatigue failure, and then discuss the specific failure process models employed and the approximation made encoding them into a computer simulation of microcrack growth.

Microscopic Failure Sequence

Three major processes can influence the fatigue lifetime and scatter in lifetime of structural alloys: (1) microcrack nucleation; (2) early microcrack growth, and (3) microcrack coalescence. These sequential events comprise the initation stage of the fatigue failure process and precede the formation of a terminal macrocrack whose subsequential progress can be predicted by fracture mechanics. Our modeling is presently constructed to describe fatigue failure wherein crack nucleation is at or near the surface at particles. It is therefore, an analog of failure of peak hardness or overaged 2000 and 7000 series aluminum alloys, which contain intermetallic particles of sufficient size to enhance nucleation rates substantially above crystallographic or at grain boundary cracking. The simulation describes a material relieved of long range residual surface stress, having no major subsurface defects, and currently also ignores the effect of triaxially of the applied stress on the initiation process. With no gross subsurface defects and no macroscopic residual surface stress, the absence of a bulk constraint of microplastic deformation during fatigue ensures that crack nucleation occurs at or near the surface.

Fatigue failure is a statistically influenced process and the scatter in lifetime can arise from fluctuations in each of the three microscopic types of failure events comprising initiation. One expects the relative contribution of the three processes to scatter in lifetime to be principally a function of the number and density of microcracks on a specimen. Thus if the cyclic stress amplitude is sufficiently small (high cycle fatigue) few cracks are formed, nucleation will dominate the statistics of failure. For low cycle fatigue, with multiple crack coalescence commonplace, the statistics of

coalescence is of prime importance. At an intermediate stress statistical scatter in microcrack growth can be expected to govern the statistics of failure.

General Simulation Technique

The simulation deals only with the growth of microcracks as seen from the surface. A fixed crack shape factor (depth/length) of 0.35 is assumed for all microcracks. We begin by defining a function P(N), which is the probability of nucleation of isolated cracks at intermetallic particles in an element of surface area, S, during the Nth fatigue cycle. P(N) is calculated for a specific cyclic stress and specific orientation of the material relative to the surface and to the principal stress axis. For the case of flexural fatigue, used in the present work, the stress and material orientations are constant over the entire gauge section of the specimen, and so S is simply the surface area of the specimen. Calculation of P(N) for more complex components requires that the surface be divided into elements of approximately constant material orientation and cyclic stress amplitude.

For each specimen fatigue lifetime to be simulated, P(N) is used with a random number selection procedure to define the cycles N_i at which the i^{th} crack nucleates with a sequential ordering so that $N_{i+1} > N_i$. Next, for each nucleation event, we determine, by random selection, the width of the intermetallic W_i from which nucleation takes place (Fig. 3), the width of the grain containing the intermetallic, G_i, and the distance of the intermetallic from the grain boundary, Z_i.(Fig. 28) There are specific constraints on the range of values of W_i, G_i, and Z_i which can occur for a given N which arise from the mechanism of nucleation as discussed later. Change in microcrack length with increment in fatigue cycles ΔN is described by

$$\Delta c = \Delta N \, A \, (\Delta K_{eff})^m \quad , \tag{16}$$

where c is the half crack length, m and A are material constants and ΔK_{eff} is an effective stress intensity range. $\Delta K_{eff} \propto (\sigma_{max} - \sigma_{cc})$, the maximum cyclic

SC79-3496

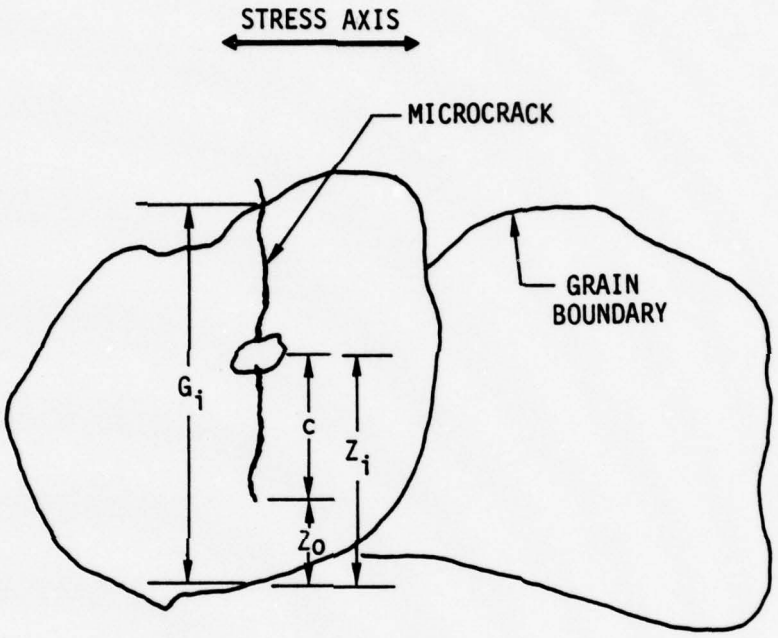

Fig. 28 Schematic illustration of surface section, defining microstructural parameters important to crack nucleation and growth.

stress minus the crack closure stress. σ_{cc} is determined from rules which relate the closure stress to the instantaneous location of a microcrack relative to surrounding microstructure.

Simulation of growth of the i^{th} crack begins for $N = N_i$ with the crack length $2c = W_i$. An incremental change in 2c is calculated for each half of the crack using Eqn. (16). The new 2c is used to determine a new ΔK_{eff}, for $N = N + \Delta N$, and the simulation of propagation continues in that manner. For crack $i = 1$, growth is continued until 2c reaches a critical size c_r at which point we set the cycles to specimen failure $N_F = N$. The second crack then is followed beginning at N_2 cycles and N is compared to N_F, and 2c to c_r. If 2c reaches c_r with $N < N_F$ the new N_F becomes the N value of the second crack. The above procedure is terminated when, for the i^{th} crack, $N_i < N_F$. During crack growth the size of grains neighboring the nucleation site are determined as needed, just as propagation of a crack tip into a new grain begins. The width of the new grain is selected at random using the distribution in width of grains normal to the stress axis. Crack coalescence is handled in much the same manner, by first defining the probability function of nucleation of cracks in grains of close proximity. The cycles to nucleation of each crack is selected along with the initial parameters describing the nucleation site sizes and locations. Propagation of each crack is then simulated to the point of coalescence, and beyond as necessary.

Single Crack Nucleation and Growth

In the present paper we compare predicted to measured parameters for isolated cracks and hence, defer discussion of simulation of crack coalescence to later reports. The nucleation phenomenon is best simulated with a two-dimensional model. For this initial effort, however, we chose to use a one dimensional simulation of the nucleation process. This provided substantial savings in computation time. We rationalized the approximation on the basis that the closure stress distribution of interest is especially sensitive to the crack growth rather than to the nucleation simulation. For purposes of comparison, we describe the approaches for both the one- and two-dimensional

simulations of crack nucleation, which aids in definitions of simplifying approximations made in the one-dimensional simulation. We begin with a general description of the nucleation process to be modeled.

Crack Nucleation: We use as a basic equation describing cycles to nucleation at a surface particle an expression proposed by Chang et.al.[R2]

$$N = \frac{C_o}{\sqrt{W}D(\sigma_{max} - \sigma_o)^2} \quad . \tag{17}$$

With reference to Fig.28, N is the number of cycles to onset of crack propagation from a particle into the matrix, W is the width of the particle normal to the stress axis, D is the largest surface slip distance (at 45° to the principal stress) within the grain containing the particle, σ_{max} is the peak cyclic stress amplitude, and C_o and σ_o are material constants. The expression pertains to fully reversed constant amplitude loading, and with simplifying assumptions describes the effect of increasing strain energy density at a nucleation site which accrues with cyclic microplastic deformation. Equation (17) defines a lower bound, in that for a particle with a given W,D and σ_{max} it predicts the minimum value of N at which cracking into the matrix will occur. Crystallographic orientation of the grains was ignored in derivation of (17) and less favorable orientations are one factor leading to scatter of nucleation to large N values.

Consider the progression of nucleation one typically observes with Al 2219-T851,[D12] wherein the nucleation sites are at intermetallic particles. During fatigue the first nucleations occur at the largest intermetallics located in large grains permitting the largest possible values of D (D_{max}). The minimum possible cycles to the first nucleation is $N_{min} = C_o/(\sqrt{W_{max}}\ D_{max}\ (\sigma_{max} - \sigma_o)^2)$. As N increases, additional nucleation events occur for intermetallics corresponding to progressively smaller values of W and D. For a given N the smallest intermetallic permitting nucleation is $W_{min} = C_o^2/(N\ D_{max}(\sigma_{max} - \sigma_o)^2)^2$. One actually observes nucleation for all particle sizes $W_{max} > W > W_{min}$. This is in part because crystallographic

orientation effects nucleation at surface particles, but is also because variation in the internal structure from one intermetallic to the next influences nucleation. The percentage of specimen surface area in which nucleation is possible is identically zero at $N = N_{min}$, and increases with increasing N - initially as portions of the largest grains in the alloy neighboring the grain boundaries become potential areas for nucleation.

Two-Dimensional Nucleation Expression: The crack nucleation phenomena we wish to simulate is most accurately described by a two-dimensional model. For point of reference, we describe briefly a two-dimensional procedure to determine the number of fatigue cycles for successive nucleation of cracks on the surface of a simulated test specimen. We assume a random distribution of intermetallic sizes over the surface. The probability of nucleation per fatigue cycle P(N) is, then, calculated from the distribution in possible slip distances, $A_\theta(D)$, and the distribution in intermetallic sizes, F(W). F(W) is the number of intermetallics per unit area with width W normal to the principal stress. $A_{+45°}(D)$ and $A_{-45°}(D)$ are normalized (to unity) relative probability distributions of finding a cord length, D, across a grain at +45° and -45° from the stress axis respectively. P(N) is simply taken to be proportional to the number of intermetallics available for fracture as defined by the limits of (17).

$$P(N) = S\, C_p \sum_{\theta=+45,-45} \int_{W_{min(N)}}^{W_{max}} F(W) \left[\int_{D_{min(N,W)}}^{D_{max}} \frac{(D - D_{min})}{D} A_\theta(D)\, dD \right] dW. \quad (18)$$

In writing (18) we have assumed that there is no substantial saturation of nucleation for any intermetallic size, i.e., that few particles of any given size fracture during fatigue - even those that are located in grains having the most favorable orientations. S is the specimen surface area, C_p is the probability of nucleation per cycle at a particle meeting the condition for nucleation defined by (17). Currently, C_p must be determined experimentally. $D_{min} = C_o/(N\sqrt{W}(\sigma_{max} - \sigma_o)^2)$.

One-Dimensional Nucleaton Expression: Using the same notation as above we set

$$P(N) = SC_p \int_{D_{min}(W = 20\ \mu m, N)}^{D_{max}} A(D)\ dD \left[\int_{10\ \mu m}^{W_{max}} f(W)\ dW \right] \qquad (19)$$

We take A(D) to be the normalized distribution in grain widths normal to the principal stress axis - which is equivalent to a simulation in which the grains are equiaxial in the plane of the surface. In calculating D_{min} we use a fixed intermetallic width of W = 20 μm, corresponding to an average of the size of intermetallic for which nucleation occurs in the 7075 alloys to be simulated. Using (19) the cycles N_i, at which a sequence of cracks i = 1,300 are nucleated, are selected randomly.

The width of the grain, G_i, in which the i^{th} crack nucleates is then chosen using A(D) for $D > D_{min}$ (w = 20 μm, $N = N_i$). We define a random number $0 \leq R \leq 1$,

$$R = \frac{\int_{D_{min}}^{G} A(D)\ dD}{\int_{D_{min}}^{D_{max}} A(D)\ dD}\ , \qquad (20)$$

and by inversion a function

$$G = X(R), \qquad (21)$$

from which G_i is chosen by random selection of R. Finally the location of the intermetallic, Z_i, within the grain is chosen at random, by assuming any location in the grain of initiation is equally likely.

With respect to a two-dimensional simulation the one-dimensional approximation has the following defects.

1) It overestimates the absolute numbers of nucleations which occur, although not necessarily the relative change in P(N) with N.

2) For $N \approx N_{min}$ it permits nucleation in the center of large grains where they are only observed at the periphery of the grains.

3) An average value of intermetallic width, and hence, initial crack size is used.

Early Crack Growth: The initial crack length (2c) is set to 20 μm for all nucleation events. For the i^{th} crack, grain width G_i and location of the nucleation site Z_i are defined as described above. If propagation into a neighboring grain occurs during growth of any microcrack, the neighboring grain width is selected at random from A(D), (i.e. the width of the grain is found using (21) for $D_{min} = 0$ in (20).

Change in crack length versus ΔN for each crack is found using (16) with the deterministic parameter being the closure stress σ_{cc}, used to calculate ΔK_{eff}. We recognize three mechanisms which can give rise to σ_{cc}, of which residual tensile strain at the microcrack tip is of most importance, and is the only mechanisms simulated here.[D8] The neglected mechanisms involve contact of opposing fracture surfaces, and pertain only when σ_{cc} is small or if $2c \approx W$. Residual tensile strain at the crack tip gives rise to σ_{cc} described by:

$$\sigma_{cc} = \frac{\alpha z_o}{2c} F(R) \sigma_{max} \qquad (22)$$

for cracks within the grain of nucleation, and

$$\sigma_{cc} = \frac{\alpha z_o}{2c} \sigma_{max} \qquad (23)$$

for cracks beyond the grain of nucleation.[D10] α is a material constant. z_o is the distance of a crack tip to the next grain boundary as illustrated by Fig. 7. Function F(R) has values lying between zero and unity.

Thus, as represented by Eqns. (22) and (23) the crack closure stress varies with microcrack propagation with largest values encountered as a crack tip enters into a new grain. F(R) is included to account for the fact that crystallographic propagation, which more likely occurs within the grain in which a crack nucleates, is often associated with lower values of closure stress. For the 7075 alloys to be modeled we set F(R) = R where $0 < R < 1$. A final constraint used on Eqns. (22) and (23) occurs if the calculated value of $\sigma_{cc} > \sigma_{max}$, in which case we set $\sigma_{cc} = \sigma_{max}$.

To begin the growth simulation for the i^{th}, crack F(R) is selected at random and σ_{cc} is calculated for each of the two surface crack tips using Eqn. (22). In the event that the intermetallic overlays a grain boundary F(R) is found independently for each crack tip. Once propagation into a neighboring grain begins, Eqn. (23) is used to calculate σ_{cc}. The values of σ_{cc} are updated for each ΔN, as 2c changes with microcrack growth.

4.1.3 EXPERIMENTAL PROCEDURES

The two Al 7075-T7 alloys utilized were taken from the same heat of material having a composition wt % 1.6 Cu, 2.5 mg, 5.6 Zn, 0.3 Cr, balance Al. The large grained alloy was in a T731 condition. The small grained alloy was prepared by a thermal mechanical process. A(D) distributions in the long transverse direction (the direction of crack propagation) for the two alloys are shown in Fig. 29. The material constant, α, for use in Eqns. (22) and (23) was obtained by comparing crack tip opening displacement to distance of the crack tip to the grain boundary using the large grained material.[D10] Flexural fatigue specimens, with a tapered design to achieve constant surface stress, were manufactured from the center of a 1.0 cm thick plate by machining

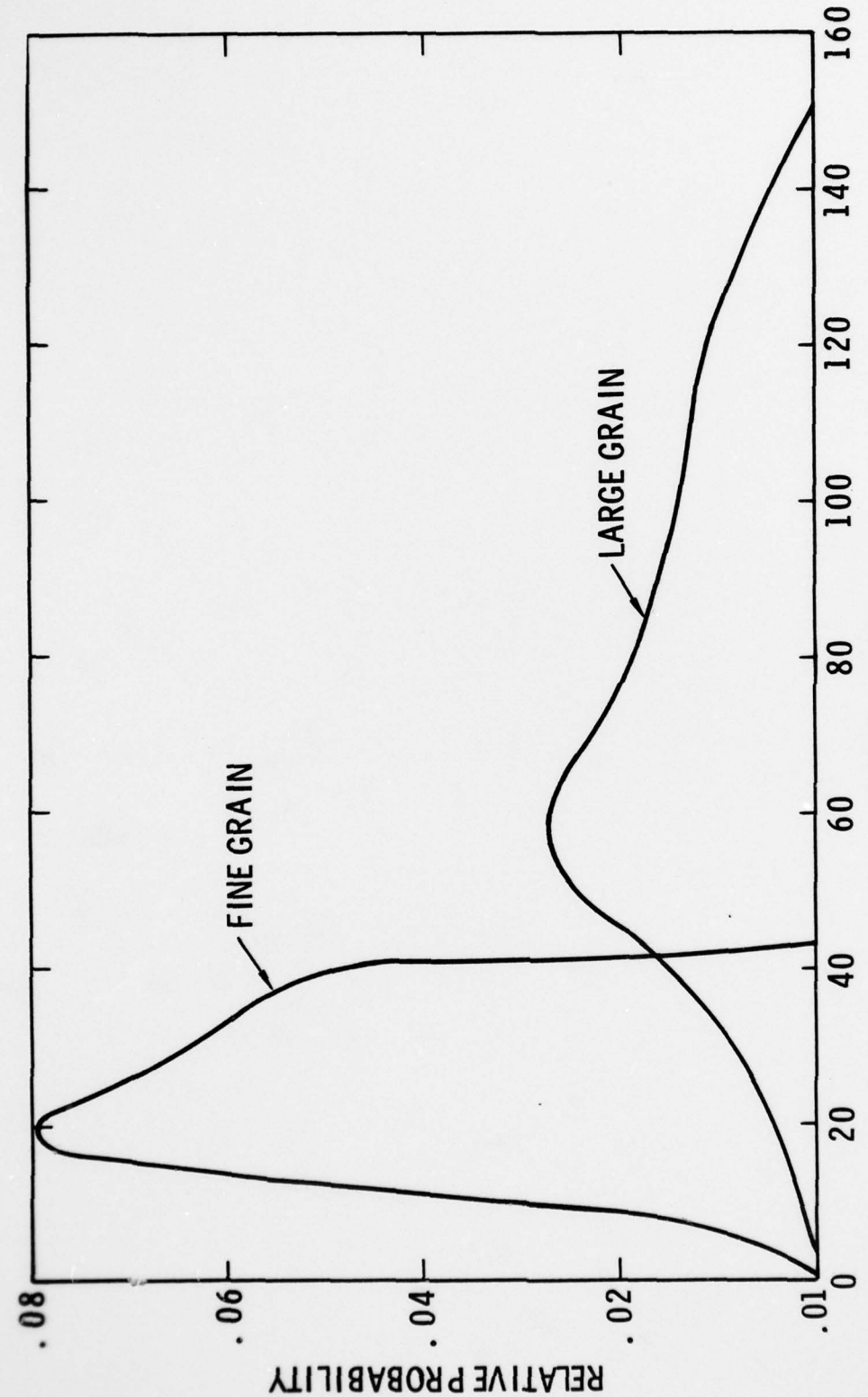

Fig. 29 Grain size distributions for the two 7075 alloys in the long transverse direction.

with decreasing cutting depths to minimize residual stress at the surface. Speciments were then mechanically polished using a 0.05 μm Al_2O_3 powder.

Fatigue loading was fully reversed with $\sigma_{max} = 0.9\ \sigma_{yield}$, in 60% relative humidity air and with the stress axis parallel to the rolling direction; it was terminated when maximum surface microcrack lengths of approximately 200 μm were achieved. The flexural fatigue geometry employed is designed for insertion into a scanning electron microscope, and using a jig in the SEM the specimen can be loaded to a desired tensile surface stress by deflecting the specimen end a measured amount.

Using a scanning electron microscope, the average closure stress of selected surface cracks was measured as a function of microcrack length. The measurement techniques have been discussed before. Briefly, they rely upon measurement of two values of crack opening displacement, from which an empirical estimate of the average closure stress, $\bar{\sigma}_{cc}$, is made.[D4]

4.1.4 RESULTS AND DISCUSSION

The computer generated predictions of $\bar{\sigma}_{cc}$ for the two grain sizes are shown in Fig. 30 and the experimentally measured values in Fig. 31. The predicted and experimental values are for isolated cracks developed by fatigue for $\sigma_{max} = 0.9\ \sigma_{yield}$. $\bar{\sigma}_{cc}$ is the average of the σ_{cc} values of the two surface crack tips for each simulated crack. A general trend towards a smaller $\bar{\sigma}_{cc}$ for the fine grained material is evident and is predicted by the model. It is also apparent that the simulation shows inadequacies of the models in three areas.

a) For short crack length the simulation predicts the occurrence of more cracks with large values of $\bar{\sigma}_{cc}$ than are actually observed. We believe the modeling problem is that closure stress is only known to affect Mode I propagation. We have observed that shear mode propagation continues into grains for which large closure stresses preclude Mode I propagation. As a consequence, microcracks are not

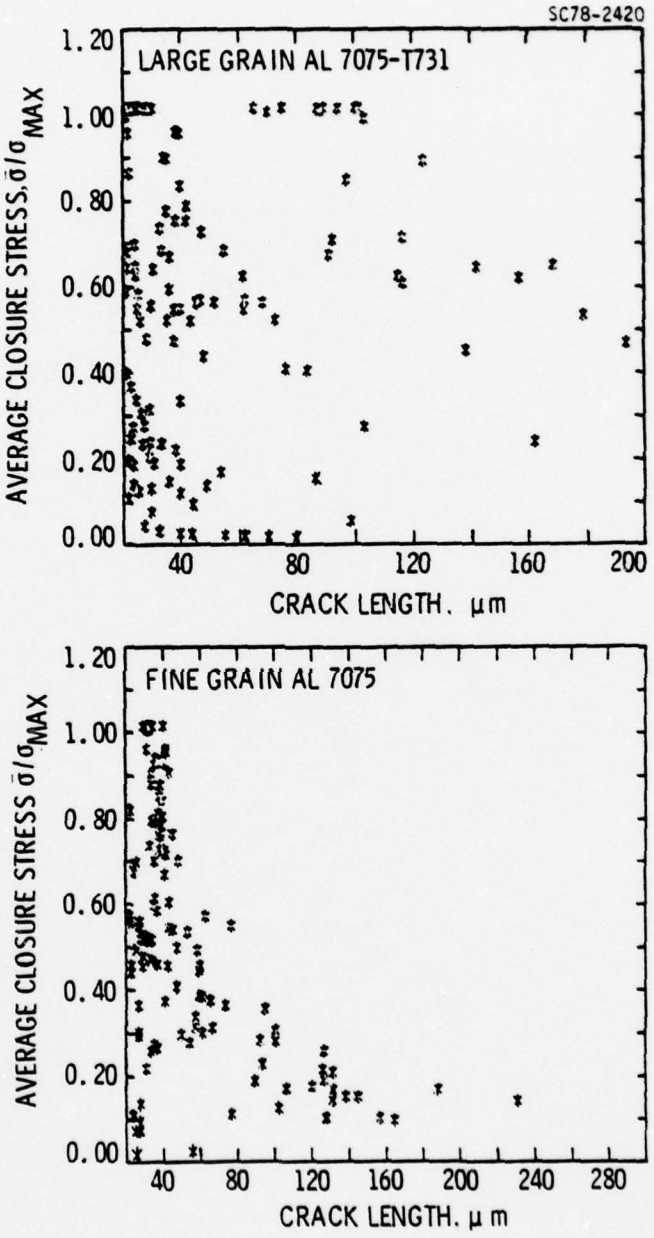

Fig. 30 Predicted values of $\bar{\sigma}_{cc}$ vs. microcrack lengths for two grain sizes. Each data point is from a different simulated microcrack.

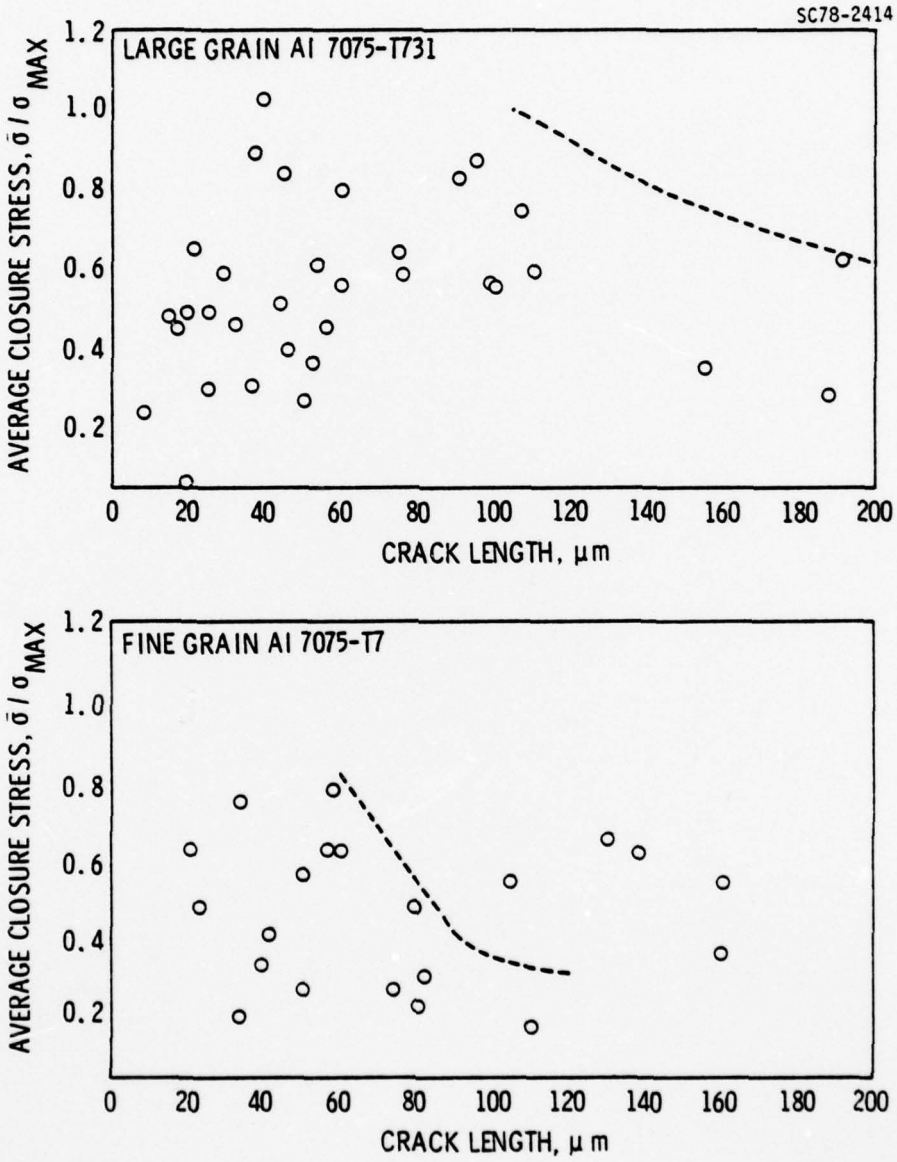

Fig. 31 Measured values of $\bar{\sigma}_{cc}$ vs. microcrack length for two grain sizes. Dash lines are upper bounds of the data from the simulation.

necessarily permanently trapped in a high closure stress condition as assumed in the simulation.

b) We expect that, for sufficient microcrack length, Eqn. (23) will fail when the crack length becomes so large that a continuum analysis is appropriate for pre prediction of the plastic zone size. The occurrence of cracks with σ_{cc} larger than expected for the fine grained material for 2c > 100μm is attributed to such an effect.

c) Experimentally, we observe no cracks for which $\bar{\sigma}_{cc} < 0.15$ σ_{max}. This is presumed to be the result of a contribution of fracture surface roughness to closure, which sets a minimum value to σ_{cc}, and which has been neglected in the present simulation.

The dashed upper bounds of the σ_{cc} values in Fig. 31 are the upper bounds from the simulation and suggest that the general trend in closure stress with crack length has been successfully modeled. Empirical modification can be made immediately to refine the models to account for items (b) and (c) above. With respect to item (a) further research is required to establish if humidity and the presence of a Mode I closure stress affects Mode II microcrack propagation.

4.1.5 SUMMARY

A Monte Carlo based computer simulation of fatigue crack initiation processes pertinent to the fatigue failure of aluminum alloys is discussed. The simulation is based upon models which describe: (1) nucleation of cracks at intermetallic particles at or near the surface, and (2) the early stage of microgrowth. An effective stress intensity range, ΔK_{eff}, is used to calculate the rates of propagation of individual cracks. In turn, the microcrack closure stress, used to determine ΔK_{eff} for a given microcrack, is determined

from a model predicting the effect of crack-tip - to grain boundary distance on closure from residual tensile strain at the crack tip.

The simulation is applied to prediction of the distribution in the average closure stress of microcracks as a function of microcrack length for two Al 7075-T7 alloys; a fine grain material with an average size of 25 μm and a large grain material having a 75 μm average grain size in the direction of crack propagation. Simulation predictions are compared to experimentally determined closure stress distributions for the two alloys. The general trends of decreasing closure stress with microcrack length for both materials, and a smaller average closure stress for the fine grained material is predicted by the simulation. The experimental data also indicate three areas in which the simulation needs improvement:

1) To allow for Mode II crack propagation for large closure stresses which limit Mode I propagation rates.

2) To describe the transition from a plastic zone size determined by grain size for smaller microcracks, to one determined by a continuum analysis for sufficiently large cracks.

3) To account for presence of a lower bound on crack closure stress resulting from a mechanism of contacting the opposing fracture surfaces behind the crack tip.

4.2 ADDITIONAL MODELING CONSIDERATIONS

Humidity: Relative humidity enters the simulation both in the nucleation and early microcrack propagation processes. One major effect of humidity is to decrease the ductility of a thin layer of material (≈5 μm) near the surface. This occurs as a consequence of cyclic loading and marks a work hardening which accompanies a penetration of some as yet undefined environmental species into the surface, presumably by a dislocation sweep-in

mechanism. The reduced surface ductility leads to a reduced probability of nucleation reflected by changes in material constants C_0 and σ_0 in the nucleation Eq. (17), and also in reduced ductility at a crack tip and hence smaller values of α in Eq. (23). These two effects are competing and one expects the net effect of humidity on fatigue lifetime of aluminum alloys will be dependent upon the distribution of intermetallic and grain sizes, as well as of the direct effect of humidity on the material coefficients.

Several additional effects of humidity must be considered in a comprehensive model: 1) Increased humidity is known to lead to an unusual weakness between intermetallic-matrix interfaces,[R1] which can further modify the behavior described by Eq. (17); 2) For cracks in fracture mechanics specimens, the environment alters the closure stress only near the crack tip. The ductility of the material at the crack tip changes with increased humidity leading to smaller σ_{cc}. However, the cyclic deformation deep within the plastic zone occurs in the absence of environmental modification and it appears, at least for certain aluminum alloys, it suffices to describe the effect of humidity using Eq. (16) by only changing σ_{cc}, with material constants A and m independent of humidity. For microcracks, at least at the surface, the entire zone of deformation is affected by the environment and hence one can expect that A, m, and σ_{cc} will all be a function of humidity, reflecting not just the effect of reduced ductility on σ_{cc} but also a change in vulnerability of the material to cyclic damage. Presently, the various material coefficients and their altered values with humidity must be determined experimentally before the simulation can proceed. If, however, in the future the coefficients are related to alloy composition and heat treatment, the fundamental predictive power of the failure simulation will be substantially increased.

Crack Coalescence in Low Cycle Fatigue

In low cycle fatigue crack nucleation density is, typically, sufficient that coalescence of microcracks becomes probable. The effect of coalescence is to reduce fatigue lifetime from that realized with isolated cracks.

The importance of an individual coalescence event depends upon the relative location of the cracks involved including the sizes of the grains in the region containing the coalescing cracks. Presently we have no model for the changes in cyclic stress intensity range which occurs when tips of microcracks enter a common grain. From fracture mechanics one expects an increase in cyclic stress intensity range. However, we know that counteracting this effect is an increase in σ_{cc} associated with larger tensile strain at the crack tips. In the simulation we make the approximation that coalescing cracks do not sense each other until their surface tips touch, at which point coalescence occurs (neglecting the effect of subsurface crack path). Presently we deal only with the coalescence of two cracks, but the procedure described below can be extended to treat multiple cracks.

Using the notation of Section 4.1 we define the probability of nucleation of a second crack in a grain neighboring a grain containing a crack developed previously, in the N^{th} cycle, over the surface area (S) element, to be

$$P'(N) = \frac{2\ P(N)}{GS} \int_{N_{min}}^{N} P(N)\ dN \quad , \qquad (24)$$

where G is the number of grains/area. The total number of single cracks in S is simply $\int_{N_{min}}^{N} P(N)\ dN$ and [2/SG] is the fraction of grains in which a second nucleation will neighbor the first (with grains aligned in the direction of crack propagation). We further modify (24) to incorporate the fact that the cracks must lie within a capture distance x (Fig. 32) if coalescence is to occur. $P_d(N)$ which results is the probability of nucleation of a second crack in a grain neighboring an already present microcrack in the N^{th} cycle and with sufficient proximity that coalescence will occur given sufficient crack propagation.

SC79-3428

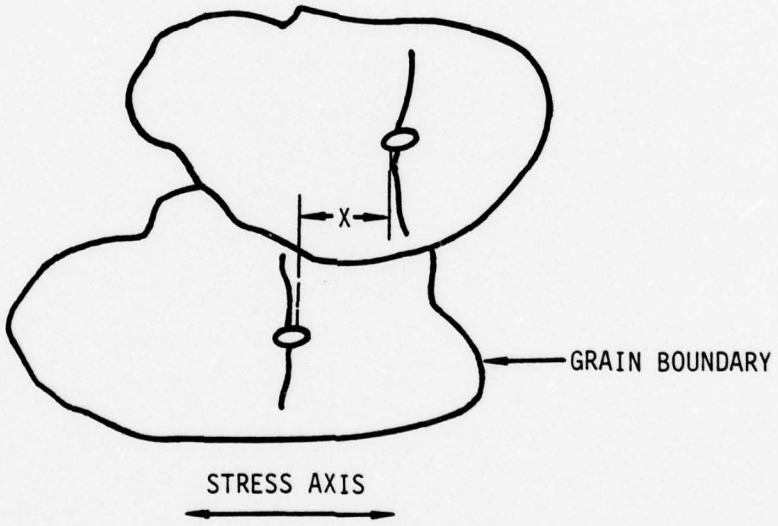

Fig. 32 Maximum nucleation site separation parallel to the stress axis for which coalescence is likely referred to as a capture distance, X.

$$P_d(N) = P'(N) \left[\int_x^{D_{max}} A_{\theta=0}(D) \frac{X}{D} \, dD + \int_0^x A_{\theta=0}(D) \, dD \right] . \qquad (25)$$

As is described in 4.1 Eq. (25) and its appropriate modifications are used to select N_i, D_i, W_i and G_i which define the nucleation parameters for the second nucleation. We then take N_i as N_{max} for the first nucleation and use the single crack equations to define the parameters for the first nucleation.

Additional probability functions are defined giving the probability of nucleation of pairs of cracks with one intervening grain, etc. The form of the probability is the same differing only in the value of x, which presently must be determined experimentally. Microcrack growth of each crack is followed as per the procedure for single cracks, until coalescence occurs at which point the growth of the unified crack is simulated.

In Fig. 33 we show an example of predicted to measured mean lifetime for the two Al 7075 alloys discussed in Section 4.1. The predictions are made using the one dimensional simulation of nucleation described earlier and a simulation incorporating potential for coalescence of two microcracks. $P_d(N) = 0$ for low cyclic strain and only single nucleation events participate in failure, but for larger cyclic strain $P_d(N) \neq 0$ and coalescence influences fatigue lifetime. The simulated data points in Fig. 33 are mean values of 100 simulated smooth bar specimens. Parameters used in the nucleation equation were selected to fit the two highest strain points for the large grain material. The predictions for the small grain alloy are a direct result of the simulation with no additional adjustable constants.

Scatter in Fatigue Lifetime

Scatter in fatigue lifetime is determined in the simulation by repeated running of the simulation for the same stress amplitude, material orientation, etc. The scatter results from statistical variations in alloy microstructure from run to run simulated by random selection governed by the grain and intermetallic size distribution functions. Our project funding

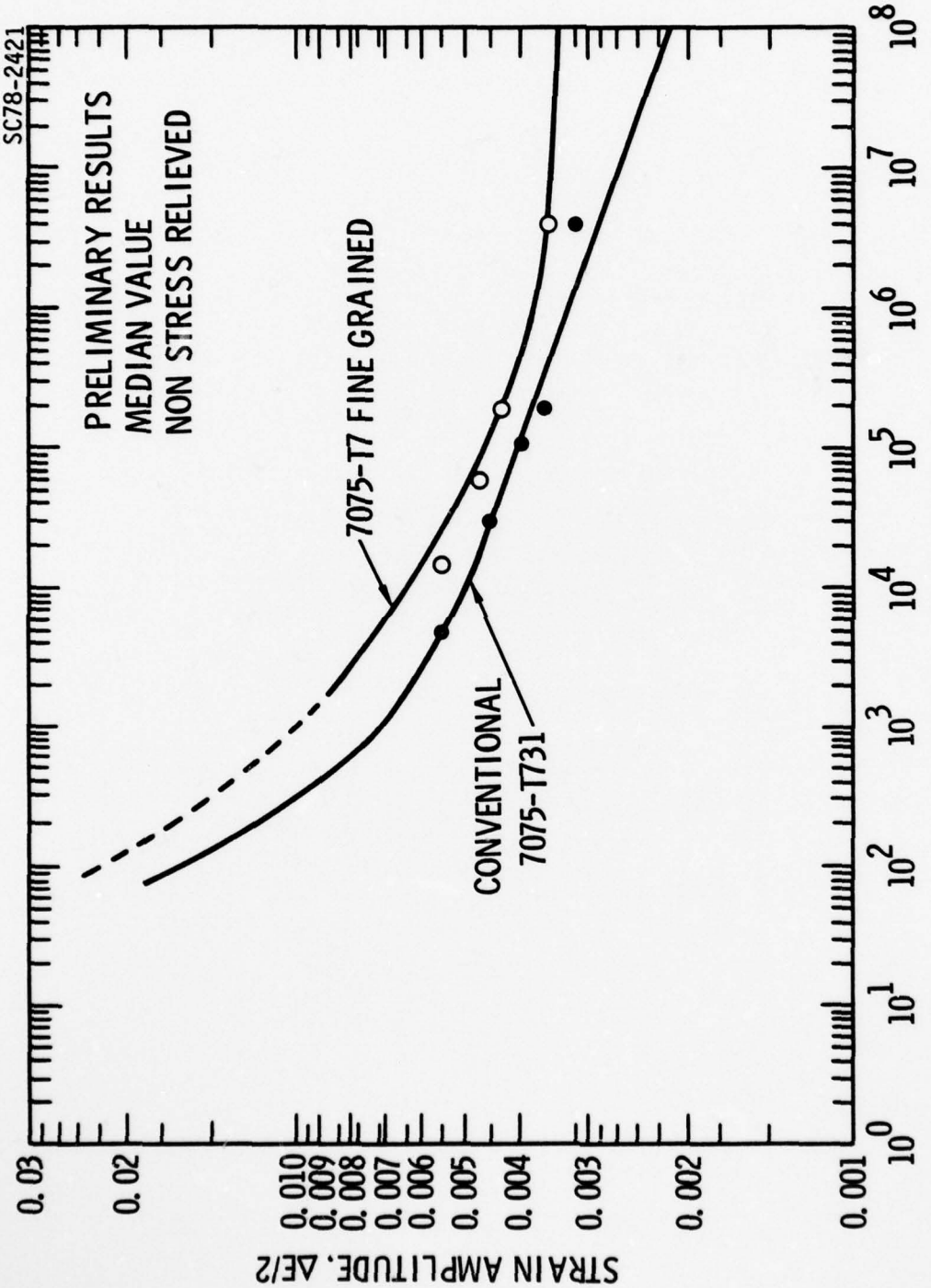

Fig. 33 Comparison of measured to predicted fatigue lifetimes for Al 7075-T7 alloys for two grain sizes.

concluded before an orderly investigation of the effect of modeling parameters on lifetime scatter could be attempted, so we have no significant results to report in this regard. Presently, we plan to defer a first test of predicted to measured lifetime scatter until a more sophisticated simulation based upon the two-dimensional nucleation model, described briefly in 4.1, is fully operational. As an addendum, however, we want to point out one interesting effect observed in the simulation of fatigue lifetime scatter illustrated by the results in Fig. 34. Lifetime in the case simulated is for high cycle fatigue involving no crack coalescence. A shift in the mean specimen lifetime is predicted with decreased specimen surface area. This "size effect" results from a decrease in sites available for nucleation, which alters the statistics of the failure process.

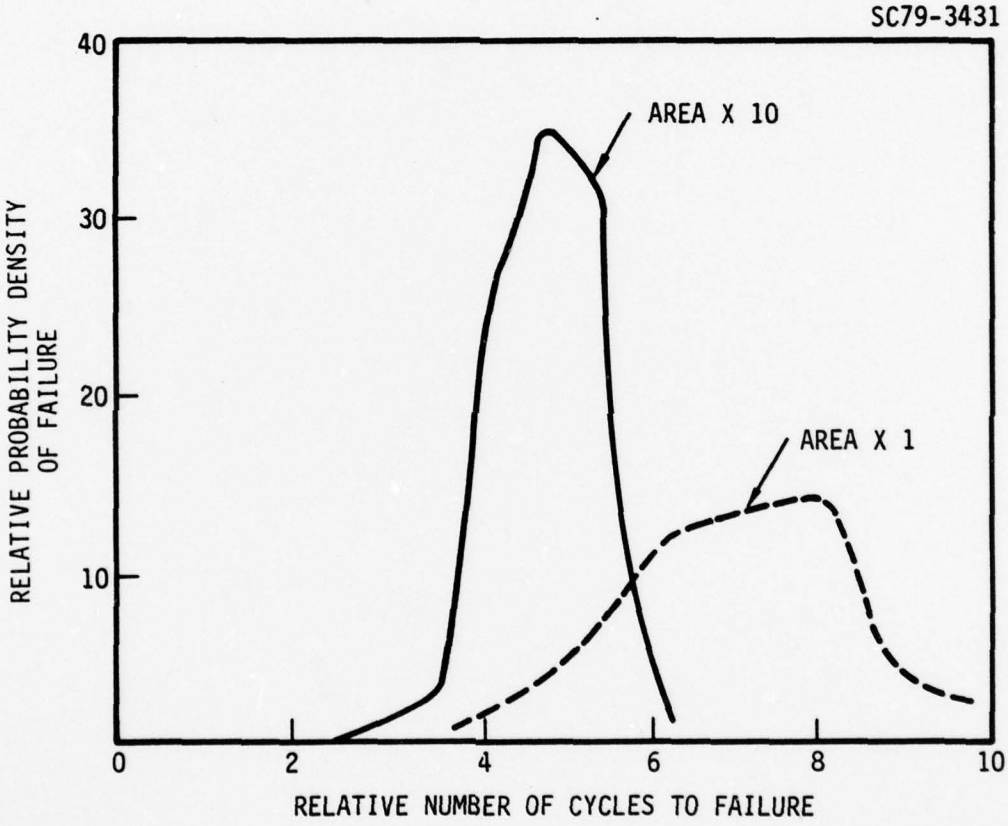

Fig. 34 Effect of surface area on simulated scatter in fatigue lifetime.

5.0 SUMMARY

A new approach to modeling of the effect of alloy microstructure and environmental factors on mean and scatter in fatigue lifetime has been reported. The Monte Carlo simulation of the fatigue failure processes described relies upon analytical models of microscopic failure processes comprising the initiation stage of fatigue failure. Comparisons between predicted and measured fatigue behavior has been encouragingly good and we can foresee that in years to come the general approach to lifetime modeling defined here will have wide applications. The main accomplishments of the research have been:

1) Test and verification of a model relating alloy grain size for 7000 and 2000 series alumninum alloys to the rate of surface crack initiation at surface particles.

2) Demonstration that crack closure stress is a principal factor governing microcrack growth in fatigued aluminum, combined with definition and verification of an analytical model relating grain size to closure stress and hence to crack propagation rate.

3) Definition of the role of humidity in several nucleation and microcrack growth processes in aluminum alloys, including development of a technique to measure the effect of humidity on the ductility of the surface.

4) Development and initial assessment of a Monte Carlo procedure to predict a) the mean and scatter in fatigue lifetime of certain aluminum alloys; b) microscopic cracking parameters of potential use to evaluation of nondestructive lifetime measurement techniques.

AD-A064 443 ROCKWELL INTERNATIONAL THOUSAND OAKS CALIF SCIENCE --ETC F/G 11/6
ENVIRONMENTAL EFFECTS ON FATIGUE CRACK INITIATION.(U)
FEB 79 W L MORRIS, O BUCK N00014-76-C-0452

UNCLASSIFIED SC5050.1FR NL

2 OF 2
AD
A064443

END
DATE
FILMED
4-79
DDC

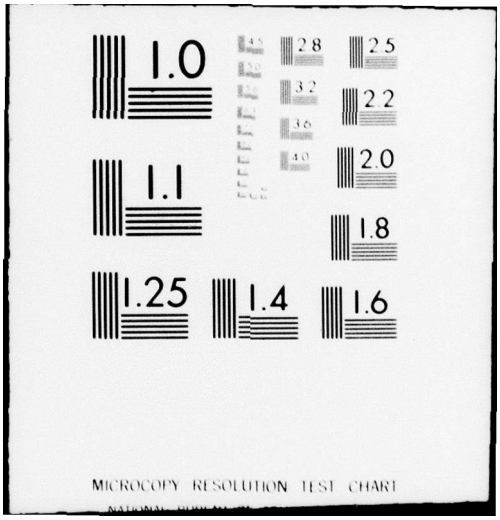
1.0
1.1
1.25
1.4
1.6
1.8
2.0
2.2
2.5
2.8
3.2
3.6
4.0
MICROCOPY RESOLUTION TEST CHART

Options to extend and refine the models and techniques described are substantial.

1) The nucleation expression can be extended to include the effect of subsurface location or triaxial stress (such at notches) on microplastic ductility and hence cycles to nucleation.

2) There is the prospect that a systematic study of the interrelationships between alloy composition, heat treatment, environmental humidity and surface ductility will lead to a method to predict the material constants used in the nucleation equation.

3) Slip distance models of the type employed for "at particle" nucleation can be formulated to describe crystallographic and at grain boundary nucleation, and tested.

4) With respect to microcrack growth, computer simulation of cyclic deformation in a plastic zone confined to the grain at a microcrack tip should provide substantial insight into the interrelationships between alloy properties, humidity, and the material constants which appear in the closure stress equations.

5) Methods to describe shear mode propagation such as in the presence of large Mode I closure stress must be developed.

6) Substantial investigation to develop models of crack coalescence with crack tips in common grains is required and should concentrate on the complex changes in closure stress in the region of interaction which are known to occur.

Comparison of Monte Carlo generated coalescence rates to measured ones can be used to refine the description of the coalescence process as initial models are developed.

7) Opportunities to test and refine the Monte Carlo simulation abound - considering that a more sophisticated simulation can include two-dimensional nucleation modeling incorporating effects of grain orientation and alloy texture, as well as orientation of the material and stress axis relative to the surface. By comparing predicted to measured fatigue properties on a microscopic level the simulation can be used to refine itself by a combination of empirical means, and by definition of areas requiring further research.

8) One approach to the nondestructive measurement of remaining fatigue lifetime is to determine (such as by acoustic harmonic generation) the distribution of microcraks on a surface. The simulation can be used to evaluate such measurement techniques.

DOCUMENTATION

Listing of papers acknowledging ONR support on Contract N00014-76-C-0452.

D1. W. L. Morris: Met. Trans., 1978, Vol. 9A, pp. 1345-1348.

D2. W. L. Morris, R. Chang and O. Buck: "Effect of Nucleation Site Size and Slip Distance on Nucleation of Cracks from Surface Discontinuities in Al 2219-T851," to be submitted to Met. Trans.

D3. W. L. Morris: Met. Trans., 1977, Vol. 8A, pp. 589-596.

D4. W. L. Morris and O. Buck: Met. Trans., 1977, Vol. 8A, pp. 597-601.

D5. W. L. Morris: Met. Trans., 1977, Vol. 8A, pp. 1087-1093.

D6. W. L. Morris: Met. Trans., 1977, Vol. 8A, pp. 1079-1085.

D7. W. L. Morris: "Microcrack Closure Phenomena in Al 2219-T851," scheduled for publication in Jan 1979 Met. Trans.

D8. W. L. Morris: "Relationship of Surface Microcrack Tip Opening Displacement to Crack Closure Stress for Al 2219-T851," to be submitted to Met. Trans.

D9. W. L. Morris: "Crack Closure Stress Effects on Rate of Propagation of Surface Microcracks During Fatigue of Al 2219-T851," to be submitted to Met. Trans.

D10. W. L. Morris: "The Relationship of Crack Tip Opening Displacement to Grain Size for Microcracks in Al 2219-T851," to be submitted to Met. Trans.

D11. W. L. Morris, R. Chang, and M. R. James, "Monte Carlo Simulation of Microcrack Growth," to be submitted to Met. Trans.

REFERENCES

R1. W. L. Morris, O. Buck, and H. L. Marcus: Met. Trans., 1976, Vol 7A, pp. 1161-65.

R2. R. Chang, W. L. Morris and O. Buck: "Fatigue Crack Nucleation at Intermetallic Particles in Alloys - A Dislocation Pile-up Model," submitted to Scripta Met.

R3. J.R. Rice: "Mechanics of Crack Tip Deformation and Extension by Fatigue", Fatigue Crack Propagation, ASTM STP 415, Am. Soc. Testing Mat., pp. 247-309, 1967.

R4. G.T. Hahan, R.G. Hougland and A.R. Rosenfield: Met. Trans., May 1972, Vol. 3, pp. 1189-1201.

R5. C. Bathias and R.M. Peloux: Met. Trans., May 1973, Vol. 4, pp. 1265-1273.

R6. D.L. Davidson and J. Lankford: J. Eng. Mat. and Tech., Jan. 1975, pp. 17-23.

R7. D.L. Davidson and J. Lankford: J. Eng. Mat. and Tech., Jan. 1976, pp. 24-29.

R8. J. Newman: ASTP STP 642, Am. Soc. Test. Mat., 1978.

R9. O. Buck, J.D. Frandsen and H.L. Marcus: Eng. Fract. Mech., 1975, Vol. 7, pp. 167-71.

R10. O. Buck, J.D. Frandsen and H.L. Marcus: ASTM STP 595, Amer. Soc. for Testing and Materials, 1976.

R11. T.T. Shih and R.P. Wei: Eng. Fract. Mech., 1974, Vol. 6, pp. 19-32.

R12. W. Elber: STP 486, pp. 230, Am. Soc. Test. and Mat., Philadelphia, 1971.

R13. H. Fuhring: Int. J. Fract. Mech., 1976, Vol. 12, p. 917-919.

R14. G.G. Garett and J.F. Knott: Eng. Fract. Mech., 1977, Vol. 9, pp. 101-104.

R15. C.K. Clark and G.C. Cassatt: Eng. Fract. Mech., 1977, Vol. 9, pp. 675-688.

R16. A.E. Green and I.N. Sneddon: Proc. Cambridge Phil. Soc., 1950, Vol. 46, pp. 159-164.

R17. R.M. McKeeking: J. Mech. Phys. Solids, 1977, Vol. 25, pp. 357-381.

R18. J. Lankford and D. L. Davidson: Int. J. Fract., 1978, Vol. 14, pp. R87-89.

R19. N.J.I. Adams: Eng. Fract. Mech., 1972, Vol. 4, pp. 543-54.

R20. F. W. Smith and D. R. Sorenson: Int. J. Fract., 1976, Vol. 12, pp. 47-57.